

Fully numerical Hartree–Fock and density functional calculations. I. Atoms

Susi Lehtola

March 11, 2019

Department of Chemistry, University of Helsinki, P.O. Box 55 (A. I. Virtasen aukio 1),
FI-00014 University of Helsinki, Finland

susi.lehtola@alumni.helsinki.fi

Abstract

Although many programs have been published for fully numerical Hartree–Fock (HF) or density functional (DF) calculations on atoms, we are not aware of any that support hybrid DFs, which are popular within the quantum chemistry community due to their better accuracy for many applications, or that can be used to calculate electric properties. Here, we present a variational atomic finite element solver in the HELFEM program suite that overcomes these limitations. A basis set of the type $\chi_{nlm}(r, \theta, \phi) = r^{-1}B_n(r)Y_l^m(\hat{\mathbf{r}})$ is used, where $B_n(r)$ are finite element shape functions and Y_l^m are spherical harmonics, which allows for an arbitrary level of accuracy.

HELFEM supports nonrelativistic HF and DF including hybrid functionals, which are not available in other commonly available program packages. Hundreds of functionals at the local spin density approximation (LDA), generalized gradient approximation (GGA), as well as the meta-GGA levels of theory are included through an interface with the LIBXC library. Electric response properties are achievable via finite field calculations.

We introduce an alternative grid that yields faster convergence to the complete basis set than commonly used alternatives. We also show that high-order Lagrange interpolating polynomials yield the best convergence, and that excellent agreement with literature HF limit values for electric properties, such as static dipole polarizabilities, can be achieved with the present approach. Dipole moments and dipole polarizabilities at finite field are reported with the PBE, PBEh, TPSS, and TPSSh functionals. Finally, we show that a recently published Gaussian basis set is able to reproduce absolute HF and DF energies of neutral atoms, cations, as well as anions within a few dozen microhartrees.

1 Introduction

Thanks to decades of development in approximate functionals and computational approaches, density functional theory (DFT)^{1,2} has become the main workhorse of computational chemistry,³⁻⁵ with several new density functionals still being published every year. As atoms are the basic building block of molecules, the first test of a new density functional often is – and should be – its performance on atoms at the complete basis set (CBS) limit. However, although multiple programs are available for fully numerical Hartree–Fock (HF) and post-HF calculations on atoms, as we have recently reviewed elsewhere,⁶ the situation is not as good for DFT.

As far as we know, there are no publicly available programs for performing fully numerical DFT calculations on atoms with hybrid and/or meta-GGA functionals, especially in the presence of an electric field. This is a problem, since the ability to generate accurate data on atoms for new density functionals would greatly facilitate their assessment and development. Accurate atomic calculations may also have other uses: many density functionals have been fitted, fully or in part, to *ab initio* data on atoms. In addition, we have shown recently that fully numerical atomic density functional calculations can be used to fashion accurate and efficient initial guesses for self-consistent field (SCF) calculations on molecules, even if the molecular calculations are done with Gaussian basis sets.⁷

In the present work, we will describe the implementation of an atomic finite element solver for HF and DFT calculations, also with hybrid and meta-GGA functionals. The program called HELFEM,⁸ where the first part stands both for the electronic Hamiltonian

$$\hat{H}_{el} = -\frac{1}{2} \sum_i \nabla_i^2 - \sum_i \frac{Z}{r_i} + \sum_{i>j} \frac{1}{r_{ij}} \quad (1)$$

as well as the city and university of Helsinki where the present author is situated, is open source (GNU General Public License), is written in object-oriented C++, and takes advantage of a number of recently published open source algorithms and libraries for its capabilities. Most importantly, HELFEM is interfaced with the LIBXC library⁹ that offers access to hundreds of exchange–correlation functionals published in the literature. HELFEM supports pure and hybrid¹⁰ density functionals at the local spin-density approximation² (LDA), generalized-gradient approximation¹¹ (GGA) as well as meta-GGA¹² levels of theory. Range-separation is not supported in HELFEM at present due to reasons that will become obvious later in the manuscript. The orbitals can be fully spin-restricted, spin-restricted open-shell, or fully spin-unrestricted.

The data layout in HELFEM is deliberately similar to what is used in typical quantum chemistry programs employing Gaussian basis sets. The rationale for this is the following. First, if one wants to use the program to study symmetry breaking effects in HF and DFT, the program cannot employ symmetries, meaning that the basis set must explicitly span all angular degrees of freedom. Second, although the basis set is local, the exchange matrix is dense because the HF exchange interaction is non-local. Furthermore, as evaluations of the total energy require access to all of the elements of the density and exchange matrices, this means that the full density and Fock matrices will anyhow be necessary. Third, by the use of full, dense matrices alike Gaussian-basis programs, many functionalities, such

as the DIIS^{13,14} and ADIIS¹⁵ SCF convergence accelerators can be adopted directly from the ERKALE program.^{16,17} Furthermore, as many powerful open-source quantum chemistry programs have recently become available, interfaces to *e.g.* PSI4¹⁸ or PYSCF¹⁹ could be implemented in the future for post-HF treatments, including multiconfigurational methods, configuration interaction, and coupled-cluster theories, thanks to the easy data interface.

We present two applications of the novel code. The first application is the calculation of atoms in finite electric fields. Finite electric field calculations allow, for instance, the extraction of atomic static dipole polarizabilities, which are a well-known challenge for theoretical methods²⁰ and the best values for which have been recently reviewed by Schwerdtfeger and Nagle.²¹ Atomic static dipole polarizabilities are related to global softness and the Fukui function.²² As the molecule with the lowest static dipole polarizability tends to be the chemically most stable,²³⁻²⁵ the accuracy of static dipole polarizabilities can be considered a proxy for thermochemical accuracy. Various density functionals have been shown to outperform HF for molecular static dipole polarizabilities with hybrid functionals yielding the best results,²⁶⁻³⁰ as the error in polarizabilities typically arises from the exchange part.³⁰ Fully numerical all-electron HF results for atoms³¹⁻³⁴ and density functional results for molecules³⁵ have been reported in the literature, whereas post-HF and relativistic DFT results have been calculated using Gaussian basis sets.³⁶⁻⁴⁰ In our application, we study the Li^+ and Sr^{2+} ions with HF and show that we are able to reproduce the fully numerical HF limit values from ref. 41. In addition, we report dipole moments and polarizabilities with the LDA,⁴²⁻⁴⁴ PBE,^{45,46} PBEh,^{47,48} TPSS,^{49,50} and TPSSH⁵¹ functionals.

Our second application is the benchmark of Gaussian basis set energies for a variety of neutral, cationic, and anionic species with HF and the BHHLYP¹⁰ functional. Atomic anions are especially challenging to model with DFT.⁵²⁻⁵⁶ For instance, it has been shown that calculations on the well-bound F^- anion may require extremely diffuse basis functions with exponents as small as(!) $\alpha = 6.9 \times 10^{-9}$ to achieve converged results.⁵⁴ The use of such small exponents requires extensive modifications to the used Gaussian-basis quantum chemistry program to ensure sufficient numerical accuracy.^{54,56} In contrast, the finite element method has none of these issues: because the basis set has local support and is never ill-conditioned, calculations are extremely stable numerically. We will show below that the absolute energies reproduced by the large Gaussian basis set used in refs. 56,57 are too large by several microhartrees for most systems. The second part of the present series presents analogous applications to diatomic molecules, where the deficiencies of Gaussian basis sets are considerably more noticeable.⁵⁸

The layout of the article is the following. Next, in the Theory section, we provide a brief presentation of the finite element method as it is unfamiliar to most quantum chemists as well as summarize the variational approach, and then proceed with the calculation of various matrix elements that are necessary for HF and DFT. The Theory section is followed by a Computational details section, which describes the present implementation and details various convergence parameters that were used for the calculations. Then, the Results section begins with extensive studies of the convergence properties of the finite-element expansion for HF calculations on the noble elements, and presents applications of the program to electric properties, and to the study of the accuracy of Gaussian basis set calculations at the HF, LDA, GGA, and meta-GGA levels of theory, including hybrid functionals. The article ends with a brief Summary and Conclusions section. Atomic units are used, unless specified

otherwise. The Einstein summation convention is employed, meaning implied summations over repeated indices.

2 Theory

2.1 Finite elements

As the finite element method is not well known in computational chemistry – to our best knowledge only one book exists on the application of the method to quantum mechanics at an accessible level⁵⁹ – we will briefly describe the one-dimensional finite element method, which is used here and in the second part of the series.⁵⁸

In the one-dimensional finite element method (FEM), the problem of the global description of a function $f(r)$ is split into a number of easier problems, that is, the description of $f(r)$ within line segments $r \in [r_{\min}, r_{\max}]$ called elements. Within each element, the value of any function $f(r)$ can be approximated using n element-specific basis functions $\phi_i(r)$ also known as shape functions as

$$f(r) \approx \sum_{i=1}^n f_i \phi_i(r). \quad (2)$$

The shape functions are traditionally chosen by specifying n control points called nodes uniformly in the element including all its edges, and demanding that each of the n basis functions correspond to the value of the function f at one of these points

$$f(r_i) = \sum_j f_j \phi_j(r_i) = f_i; \quad (3)$$

the condition of equation (3) can be equally written in the form

$$\phi_i(r_j) = \delta_{ij}. \quad (4)$$

Equation (4) yields the well-known Lagrange interpolating polynomials (LIPs), which can also be written in closed form as

$$\phi_i(r) = \prod_{j=0, j \neq i}^{n-1} \frac{r - r_j}{r_i - r_j}. \quad (5)$$

Two- and three-node LIPs are shown in figure 1.

In addition to LIPs, also Hermite interpolating polynomials (HIPs) can be used. First-order HIPs are defined by

$$\phi_{2i}(r_j) = \delta_{ij}, \quad \phi_{2i+1}(r_j) = 0, \quad (6)$$

$$\phi'_{2i}(r_j) = 0, \quad \phi'_{2i+1}(r_j) = \delta_{ij}, \quad (7)$$

that is, the even and odd-numbered basis functions describe the values of $f(r)$ and $f'(r)$ at the nodes, respectively, guaranteeing continuity both of the function and its derivative across element boundaries. It has been claimed that due to this added flexibility, HIPs yield

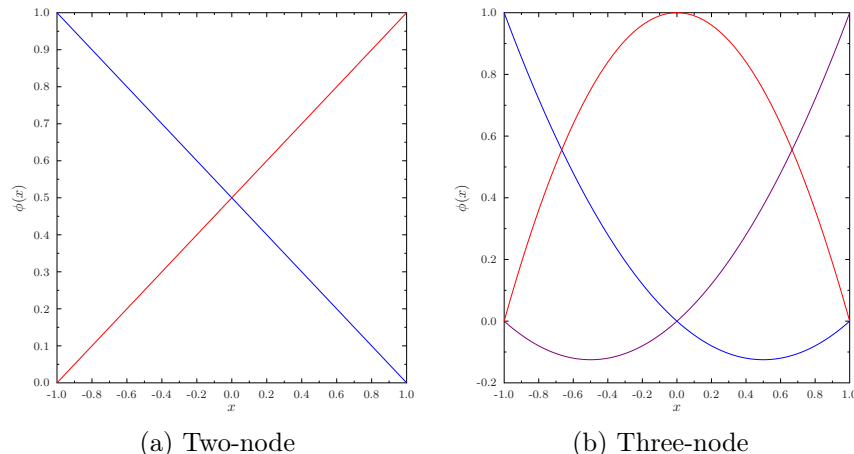


Figure 1: LIP elements with two and three uniformly spaced nodes.

better results for quantum mechanical problems than LIPs.^{59,60} Analogous expressions to equations (6) and (7) can be developed for higher order HIPs that guarantee continuity of the derivative up to the n^{th} order; LIPs being equivalent to 0^{th} order HIPs.

In order to derive expressions for HIPs, we shall follow the style of traditional finite element textbooks such as ref. 59, and write the basis functions in terms of primitive polynomials as

$$\phi_i(r) = c_{i,0} + c_{i,1}r + \cdots + c_{i,n-1}r^{n-1}. \quad (8)$$

The expansion for LIPs can be obtained by writing out equation (4) as a matrix equation

$$\begin{pmatrix} 1 & r_0 & r_0^2 & \cdots & r_0^{n-1} \\ 1 & r_1 & r_1^2 & \cdots & r_1^{n-1} \\ \vdots & \vdots & \vdots & \ddots & \vdots \\ 1 & r_{n-1} & r_{n-1}^2 & \cdots & r_{n-1}^{n-1} \end{pmatrix} \times \begin{pmatrix} c_{00} & c_{01} & c_{02} & \cdots & c_{0,n-1} \\ c_{10} & c_{11} & c_{12} & \cdots & c_{1,n-1} \\ \vdots & \vdots & \vdots & \ddots & \vdots \\ c_{n-1,0} & c_{n-1,1} & c_{n-1,2} & \cdots & c_{n-1,n-1} \end{pmatrix} = \mathbf{1}. \quad (9)$$

Denoting the first matrix in equation (9) as \mathbf{R} and the second matrix containing the primitive coefficients as \mathbf{C} , the primitive coefficients can be solved with $\mathbf{C} = \mathbf{R}^{-1}$. HIPs can be solved in terms of primitive polynomials with a matrix equation similar to equation (9); HIPs of an arbitrary order are supported in HELFEM.

Despite the use of primitive polynomial expansions in most finite element textbooks, the resulting matrix equations of the type of equation (9) become numerically unstable for high orders due to the Runge phenomenon, limiting one to polynomials of a low order, such as five or six. However, numerically stable alternatives can be fashioned by the use of orthogonal polynomials. For instance, although equation (5) is unstable with uniformly spaced nodes, it can be made stable to high orders by switching to the use of non-uniformly spaced nodes. Choosing the locations of the nodes based on a quadrature rule such as Gauss-Lobatto as in the spectral element method⁶¹ yields an especially powerful approach. An example of a six-node LIP element with Lobatto nodes is shown in figure 2a. We have also implemented another numerically stable primitive basis, similarly allowing the use of high-order elements, by following Flores *et al.*^{62,63} and using Legendre polynomials $P_n(x)$ in terms of the shape

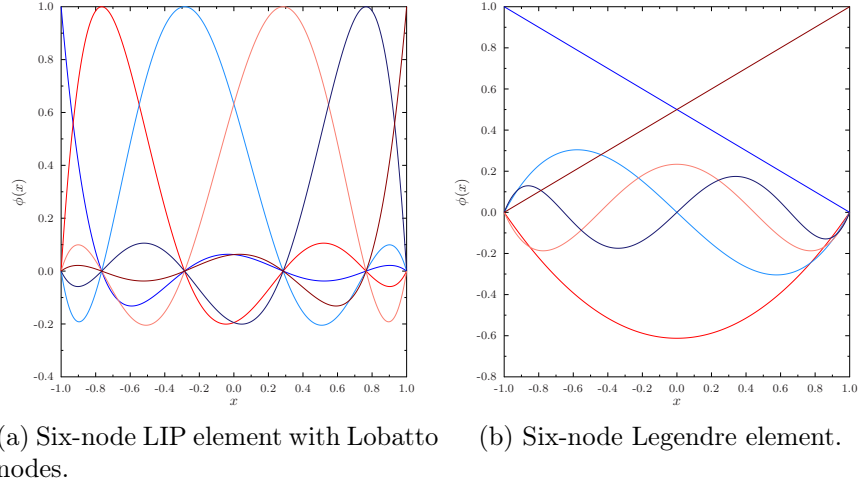


Figure 2: Numerically stable elements.

functions

$$\phi_j(x) = \frac{1}{\sqrt{4j+2}} (P_{j+1}(x) - P_{j-1}(x)), j \in [1, N-2] \quad (10)$$

that vanish at the boundaries, the first and last basis functions that guarantee continuity of the wave function across element boundaries being given by

$$\phi_0(x) = \frac{1}{2} (P_0(x) - P_1(x)), \quad (11)$$

$$\phi_{N-1}(x) = \frac{1}{2} (P_0(x) + P_1(x)). \quad (12)$$

An example of the Legendre basis is shown in figure 2b. The lowest-order Legendre element given by equations (11) and (12) is equivalent to the 2-node LIP element, whereas higher orders describe variations at smaller and smaller scales.

As only one function contributes to the value at a given node, boundary conditions can be easily implemented in the finite element approach. Orbitals can be made to vanish at the origin by removing the first basis function from the first radial element. Likewise, the vanishing boundary condition at infinity is achieved by removing the last basis function in the last radial element. Note, however, that for a HIP basis, the boundary condition of origin only applies to the function value, not any of its derivatives; at infinity both the function and its derivatives are set to zero.

2.1.1 Finite element matrices

Although the basis functions are only defined within a single element, nodes at the element boundary are shared between the functions of the two elements touching at the boundary. As a node defines a basis function, this means that the basis functions sharing the node at the boundary must be identified with each other. That is, while given three three-node LIP

employed for all values of l and m . This approach is also chosen in the present work, as the use of a common radial grid simplifies the implementation, as will also be seen below.

In the following, basis functions i carry both an angular part l_i , m_i , and a radial part B_i . The full dimension of the basis set is given by the number of radial functions times the number of angular functions.

2.3 Variational approach

As is well known, the variational solution of the HF equations within a basis set leads to the Roothaan⁶⁵ or Pople–Nesbet equations⁶⁶

$$\mathbf{F}_\sigma \mathbf{C}_\sigma = \mathbf{S} \mathbf{C}_\sigma \boldsymbol{\epsilon}_\sigma; \quad (17)$$

analogous equations are also obtained in the case of Kohn–Sham DFT.^{67,68} Here, \mathbf{F}_σ is the (Kohn–Sham) Fock operator of spin σ , \mathbf{C}_σ are the canonical molecular orbital coefficients, and $\boldsymbol{\epsilon}_\sigma$ is a diagonal matrix holding the corresponding orbital energies.

Although we have chosen the basis functions to be complex, we are free to choose the coefficients to be real in the absence of a magnetic field. Note that complex coefficients may be necessary in some approaches even in the absence of an magnetic field, see *e.g.* refs. 69–74. In contrast, the coefficients can be chosen to be real even *in the presence* of a magnetic field in the case of atoms and diatomic molecules in a parallel field; see ref. 75.

The Roothaan / Pople–Nesbet equations are solved in the present work by symmetric orthonormalization:⁷⁶ writing the unknown orbital coefficient in terms of a transformation matrix \mathbf{X} as

$$\mathbf{C} = \tilde{\mathbf{C}} \mathbf{X} \quad (18)$$

and left-multiplying equation (17) with \mathbf{X}^T , one obtains the equation

$$\mathbf{X}^\text{T} \mathbf{F} \mathbf{X} \tilde{\mathbf{C}} = \mathbf{X}^\text{T} \mathbf{S} \mathbf{X} \tilde{\mathbf{C}} \boldsymbol{\epsilon}. \quad (19)$$

Setting $\mathbf{X} = \mathbf{S}^{-1/2}$, equation (19) simplifies into a normal eigenvalue equation

$$\tilde{\mathbf{F}} \tilde{\mathbf{C}} = \tilde{\mathbf{C}} \boldsymbol{\epsilon}, \quad (20)$$

where the transformed Fock matrix is given by

$$\tilde{\mathbf{F}} = \left(\mathbf{S}^{-1/2} \right)^\text{T} \mathbf{F} \mathbf{S}^{-1/2}. \quad (21)$$

The molecular orbital coefficients in the original basis can be obtained from the solution of equation (20) with equation (18).

Because the finite element basis set is never ill-conditioned, $\mathbf{S}^{-1/2}$ for equation (19) can be constructed in HELFEM with either Cholesky factorization

$$\mathbf{S} = \mathbf{L} \mathbf{L}^\text{T}, \quad (22)$$

$$\mathbf{S}^{-1/2} = \mathbf{L}^{-1}, \quad (23)$$

or an eigendecomposition

$$\mathbf{S} = \mathbf{Q}\mathbf{\Lambda}\mathbf{Q}^T, \quad (24)$$

$$\mathbf{S}^{-1/2} = \mathbf{Q}\mathbf{\Lambda}^{-1/2}\mathbf{Q}^T. \quad (25)$$

The orthonormalization based on equations (22) and (23) or equations (24) and (25) is performed in terms of normalized basis functions, as this turns out to be necessary for the numerical stability of the procedure. However, the basis functions themselves are not normalized in HELFEM; the normalization is stored in the rows of $\mathbf{S}^{-1/2}$. As symmetry with respect to the m quantum number is used by default in HELFEM, the eigendecomposition can be blocked by m channel in solving equations (20) and (24); this makes the diagonalizations fast even in large basis sets.

2.4 One-electron matrix elements

To be able to solve the SCF equation (equation (17)), we need to compute several matrix elements. The Fock operator corresponding to spin σ is given by

$$\mathbf{F}_\sigma = \mathbf{T} + \mathbf{V}^{\text{nuc}} + \mathbf{J}(\mathbf{P}) + \mathbf{K}(\mathbf{P}_\sigma), \quad (26)$$

where \mathbf{T} is the kinetic energy, \mathbf{V}^{nuc} is the nuclear attraction, and \mathbf{J} and \mathbf{K} are the Coulomb repulsion and exchange(-correlation) matrices that contain two-electron interactions. \mathbf{P}_σ is the density matrix for spin σ

$$\mathbf{P}_\sigma = \sum_{i \text{ occupied}} \mathbf{C}_{i\sigma} \mathbf{C}_{i\sigma}^\dagger \quad (27)$$

and \mathbf{P} is the total density matrix

$$\mathbf{P} = \mathbf{P}_\alpha + \mathbf{P}_\beta. \quad (28)$$

2.4.1 Overlap

The overlap matrix elements are simply

$$S_{ij} = \langle i | j \rangle = \delta_{l_i, l_j} \delta_{m_i, m_j} \int B_i(r) B_j(r) dr, \quad (29)$$

where δ_{ij} is the Kronecker delta symbol. Here and in the following, integration over $r \in [0, \infty)$ is implied for brevity; however, the finite support of the basis functions truncate the integrals to a finite interval.

2.4.2 Kinetic energy

The evaluation of the kinetic energy matrix is slightly more complicated. In spherical coordinates, the gradient of a function f is given by

$$\nabla f = \frac{\partial f}{\partial r} \hat{r} + \frac{1}{r} \frac{\partial f}{\partial \theta} \hat{\theta} + \frac{1}{r \sin \theta} \frac{\partial f}{\partial \phi} \hat{\phi}, \quad (30)$$

where \hat{r} , $\hat{\theta}$, and $\hat{\phi}$ are unit vectors in the direction of the coordinates r , θ , and ϕ , respectively. The Laplacian reads

$$\nabla^2 f = \frac{1}{r^2} \frac{\partial}{\partial r} \left(r^2 \frac{\partial f}{\partial r} \right) + \frac{1}{r^2 \sin \theta} \frac{\partial}{\partial \theta} \left(\sin \theta \frac{\partial f}{\partial \theta} \right) + \frac{1}{r^2 \sin^2 \theta} \frac{\partial^2 f}{\partial \phi^2}, \quad (31)$$

which can be rewritten as

$$\nabla^2 f = \frac{1}{r^2} \frac{\partial}{\partial r} \left(r^2 \frac{\partial f}{\partial r} \right) - \frac{1}{r^2} \hat{L}^2 f \quad (32)$$

where \hat{L}^2 is the angular momentum operator. Thus, the kinetic energy is

$$T_{ij} = \left\langle i \left| -\frac{\nabla^2}{2} \right| j \right\rangle \quad (33)$$

$$= -\frac{1}{2} \delta_{l_i, l_j} \delta_{m_i, m_j} \int \frac{B_i(r)}{r} \left[\frac{1}{r^2} \frac{\partial}{\partial r} \left(r^2 \frac{\partial}{\partial r} \left[\frac{B_j(r)}{r} \right] \right) - \frac{l(l+1)}{r^2} \frac{B_j(r)}{r} \right] r^2 dr \quad (34)$$

$$= -\frac{1}{2} \delta_{l_i, l_j} \delta_{m_i, m_j} \int \frac{B_i(r)}{r} \left[\frac{\partial}{\partial r} (r B_j'(r) - B_j(r)) - \frac{l(l+1) B_j(r)}{r} \right] dr \quad (35)$$

$$= -\frac{1}{2} \delta_{l_i, l_j} \delta_{m_i, m_j} \int \frac{B_i(r)}{r} \left[r B_j''(r) - \frac{l(l+1) B_j(r)}{r} \right] dr \quad (36)$$

Using partial integration to move the first derivative

$$\int B_i(r) \frac{\partial^2}{\partial r^2} B_j(r) dr = \left| B_i(r) \frac{\partial}{\partial r} [B_j(r)] - \int \frac{\partial}{\partial r} [B_i(r)] \frac{\partial}{\partial r} [B_j(r)] dr, \quad (37) \right.$$

where the substitution term (first term in equation (37)) vanishes since the basis functions and their derivatives are zero at the end points, one obtains the final expression

$$T_{ij} = \frac{1}{2} \delta_{l_i, l_j} \delta_{m_i, m_j} \left[\int B_i'(r) B_j'(r) dr + l(l+1) \int r^{-2} B_i(r) B_j(r) dr \right]. \quad (38)$$

The $l(l+1)/r^2$ term in equation (38) implies that non- s states must vanish at the origin, as otherwise the kinetic energy would go to infinity. However, as the r^{-1} factor has been included explicitly in the basis set (equation (16)), we must require that $B_n(r)$ has to go to zero at the origin also for s states – meaning the radial basis set is identical for all values of l and m – as otherwise the value of the orbital $r^{-1} B_n(r)$ would diverge at the nucleus.

The $l(l+1)/r^2$ term is also responsible for the energy ordering of atomic shells. As discussed in ref. 7, the term prevents p , d , and f orbitals from seeing the less-screened regions of the nuclear potential close to the nucleus, thereby causing the orbitals with $l > 1$ to lie higher in energy than what would be statically expected just from the $l(l+1)/r^2$ term itself.

2.4.3 Nuclear attraction

The nuclear attraction matrix for a point nucleus is

$$V_{ij}^{\text{nuc}} = \left\langle i \left| -\frac{Z}{r} \right| j \right\rangle \quad (39)$$

$$= -Z \delta_{l_i, l_j} \delta_{m_i, m_j} \int r^{-1} B_i(r) B_j(r) dr. \quad (40)$$

2.5 Quadrature

Although the integrals can in principle be computed analytically in a primitive polynomial basis, the polynomials would need to be translated to the location of the element, which we have found to be numerically problematic. Furthermore, as the use of primitive polynomials is numerically unstable, like other FEM programs, we choose to calculate the integrals using quadrature, as this allows the basis functions to be chosen freely. Gauss–Chebyshev quadrature on the primitive interval $x \in [-1, 1]$ is employed in HELFEM, as the integration nodes and weights have closed-form expressions. The necessary coordinate transformation from $r \in [r_{\min}, r_{\max}]$ to $x \in [-1, 1]$ is given by

$$r = r_0 + \lambda x \quad (41)$$

where

$$r_0 = \frac{r_{\max} + r_{\min}}{2} \quad (42)$$

is the midpoint of the interval and

$$\lambda = \frac{r_{\max} - r_{\min}}{2} \quad (43)$$

is its length. Using the transformation in equation (41), the necessary quadrature rules are obtained as

$$\int r^n B_1(r) B_2(r) dr \approx \lambda \sum_i w_i r(x_i)^n B_1(x_i) B_2(x_i) \quad (44)$$

$$\int \frac{\partial B_1}{\partial r} \frac{\partial B_2}{\partial r} dr \approx \lambda^{-1} \sum_i w_i B_1'(x_i) B_2'(x_i) \quad (45)$$

2.6 Two-electron integrals

The two-electron integrals

$$(ij|kl) = \int \frac{\chi_i(\mathbf{r}) \chi_j^*(\mathbf{r}) \chi_k(\mathbf{r}') \chi_l^*(\mathbf{r}')}{|\mathbf{r} - \mathbf{r}'|} d^3r d^3r' \quad (46)$$

can be evaluated with the help of the Laplace expansion

$$\frac{1}{r_{12}} = \frac{4\pi}{r_{>}} \sum_{L=0}^{\infty} \frac{1}{2L+1} \left(\frac{r_{<}}{r_{>}} \right)^L \sum_{M=-L}^L Y_L^M(\Omega_1) (Y_L^M(\Omega_2))^*, \quad (47)$$

where $r_<$ and $r_>$ denote the smaller and greater of r_1 and r_2 , respectively, as

$$\begin{aligned}
(ij|kl) &= \int dr_1 dr_2 B_i(r_1) B_j(r_1) B_k(r_2) B_l(r_2) \\
&\times \frac{4\pi}{r_>} \sum_{L=0}^{\infty} \frac{1}{2L+1} \left(\frac{r_<}{r_>} \right)^L \int d\Omega_1 d\Omega_2 \sum_{M=-L}^L Y_L^M(\Omega_1) (Y_L^M(\Omega_2))^* \\
&\times Y_{l_i}^{m_i}(\Omega_1) (Y_{l_j}^{m_j}(\Omega_1))^* Y_{l_k}^{m_k}(\Omega_2) (Y_{l_l}^{m_l}(\Omega_2))^*
\end{aligned} \tag{48}$$

Invoking the rule of complex conjugation of spherical harmonics

$$(Y_l^m(\Omega))^* = (-1)^m Y_l^{-m}(\Omega) \tag{49}$$

and employing their closure relation

$$Y_{l_1}^{m_1}(\Omega) Y_{l_2}^{m_2}(\Omega) = \sum_{LM} G_{l_1 l_2, M}^{m_1 m_2, L} Y_L^M(\Omega) \tag{50}$$

where an asymmetric definition for the Gaunt coefficient is used⁷⁷

$$G_{l_1 l_2, M}^{m_1 m_2, L} = (-1)^M \sqrt{\frac{(2L+1)(2l_1+1)(2l_2+1)}{4\pi}} \begin{pmatrix} l_1 & l_2 & L \\ m_1 & m_2 & -M \end{pmatrix} \begin{pmatrix} l_1 & l_2 & L \\ 0 & 0 & 0 \end{pmatrix} \tag{51}$$

the two-electron integral is obtained in the form

$$\begin{aligned}
(ij|kl) &= \int dr_1 dr_2 B_i(r_1) B_j(r_1) B_k(r_2) B_l(r_2) \\
&\times \frac{4\pi}{r_>} \sum_L \frac{1}{2L+1} \left(\frac{r_<}{r_>} \right)^L G_{L l_i, m_j}^{M m_i, l_j} G_{L l_i, m_k}^{M m_l, l_k}.
\end{aligned} \tag{52}$$

From equation (52), it is seen that the integral is non-zero only if

$$L_{\min} \leq L \leq L_{\max} \tag{53}$$

and

$$m_j - m_i = M = m_k - m_l, \tag{54}$$

where

$$L_{\min} = \max\{|l_i - l_j|, |l_k - l_l|\}, \tag{55}$$

$$L_{\max} = \min\{l_i + l_j, l_k + l_l\}. \tag{56}$$

Furthermore, as the spherical harmonic with quantum numbers L and M must exist in order for the coupling to make sense, one obtains the further condition

$$L_{\min} \geq |M|. \tag{57}$$

The conditions in equations (53) to (57) truncate the series in equation (52) to a finite number of terms. Thus, the repulsion integrals reduce to the simple expression

$$(ij|kl) = \sum_{L_{\min}}^{L_{\max}} I_{ijkl}^L G_{Ll_i, m_j}^{Mm_i, l_j} G_{Ll_i, m_k}^{Mm_i, l_k} \quad (58)$$

where M is defined via equation (54) and the primitive integrals are defined as

$$I_{ijkl}^L = \frac{4\pi}{2L+1} \int dr_1 dr_2 B_i(r_1) B_j(r_1) B_k(r_2) B_l(r_2) \frac{r_1^L}{r_2^{L+1}}. \quad (59)$$

2.6.1 Primitive integrals

The primitive integrals can be split into two terms

$$\int dr_1 dr_2 f(r_1) g(r_2) \frac{r_1^L}{r_2^{L+1}} = \int_0^\infty dr_1 \int_0^{r_1} dr_2 f(r_1) g(r_2) \frac{r_2^L}{r_1^{L+1}} + \int_0^\infty dr_2 \int_0^{r_2} dr_1 f(r_1) g(r_2) \frac{r_1^L}{r_2^{L+1}} \quad (60)$$

$$= \int_0^\infty dr_1 \int_0^{r_1} dr_2 f(r_1) g(r_2) \frac{r_2^L}{r_1^{L+1}} + \int_0^\infty dr_1 \int_0^{r_1} dr_2 f(r_2) g(r_1) \frac{r_2^L}{r_1^{L+1}} \quad (61)$$

$$= \int_0^\infty dr_1 \int_0^{r_1} dr_2 [f(r_1)g(r_2) + f(r_2)g(r_1)] \frac{r_2^L}{r_1^{L+1}} \quad (62)$$

as the integration over r_1 and r_2 can be divided into integration over two triangles separated by the line $r_1 = r_2$. Substituting equation (62) into equation (59) yields

$$I_{ijkl}^L = \frac{4\pi}{2L+1} \int_0^\infty dr_1 r_1^{-L-1} B_i(r_1) B_j(r_1) \int_0^{r_1} dr_2 r_2^L B_k(r_2) B_l(r_2) \quad (63)$$

$$+ \frac{4\pi}{2L+1} \int_0^\infty dr_1 r_1^{-L-1} B_k(r_1) B_l(r_1) \int_0^{r_1} dr_2 r_2^L B_i(r_2) B_j(r_2) \quad (64)$$

As the basis functions have finite support, the functions i and j have to reside in the same element, and the functions k and l have to reside in the same element, as otherwise their product vanishes.

If ij and kl are *not within* the same element, then only a single term in equation (64) survives

$$I_{ijkl}^L = \frac{4\pi}{2L+1} \left[\int_{ij \text{ element}} dr_1 r_1^{-1-L} B_i(r_1) B_j(r_1) \right] \left[\int_{kl \text{ element}} dr_2 r_2^L B_k(r_2) B_l(r_2) \right] \quad (65)$$

and this interelement integral factorizes into two simple radial integrals with indices ij and kl . We have assumed in equation (65) that ij are farther from the origin than kl .

If ij and kl are *within* the same element, one has to evaluate the intraelement primitive integral from equation (64). This proceeds in three steps:

$$\phi_{kl}^L(r) = \int_0^r dr' r'^L B_k(r') B_l(r'), \quad (66)$$

$$[ij|kl]^L = \int_0^\infty dr r^{-L-1} B_i(r) B_j(r) \phi_{kl}^L(r), \quad (67)$$

$$I_{ijkl}^L = \frac{4\pi}{2L+1} ([ij|kl]^L + [kl|ij]^L). \quad (68)$$

Note that the integral in equation (66) does not range over the whole element, *i.e.* it only involves *part* of the basis functions. As the outer integral equation (67) is performed using quadrature with quadrature points $r_i, i \in [1, N]$, the inner integral equation (66) is evaluated in slices by

$$\phi_{kl}^L(r_i; r_{i-1}) = \int_{r_{i-1}}^{r_i} dr' r'^L B_k(r') B_l(r') \quad (69)$$

from which the full integral is recovered with

$$\phi_{kl}^L(r_i) = \begin{cases} \phi_{kl}^L(r_1; 0) & j = 1 \\ \phi_{kl}^L(r_j; r_{j-1}) + \phi_{kl}^L(r_{j-1}) & j > 1 \end{cases} \quad (70)$$

Denoting the number of primitive basis functions per element as N_p and the number of elements as N_{el} , the storage of the two-electron integrals then requires $2(L_{\text{max}} + 1)N_p^2 N_{\text{el}}$ memory for the interelement integrals, and $(L_{\text{max}} + 1)N_p^4 N_{\text{el}}$ memory for the intraelement integrals, where the maximum possible angular momentum is $L_{\text{max}} = 2l_{\text{max}}$. Importantly, the scaling of the storage cost is bilinear in the number of elements and in the angular grid, implying that large expansions can be employed.

2.6.2 Coulomb matrix

The Coulomb matrix is given by

$$J_{ij} = \sum_{kl} (ij|kl) P_{kl}. \quad (71)$$

Insertion of the two-electron integrals (equation (58)) gives the Coulomb matrix in the form

$$J_{ij} = \sum_{L_{\text{min}}}^{L_{\text{max}}} G_{Ll_i, m_j}^{Mm_i, l_j} I_{ijkl}^L \left(P_{kl} G_{Ll_1, m_k}^{Mm_1, l_k} \right). \quad (72)$$

Because the primitive integrals I_{ijkl}^L only depend on the radial part, the Coulomb matrix can be formed in three steps:

1. contract the density matrices into radial-only auxiliary matrices $P_{kl}^{LM} = \sum_{kl} P_{kl} G_{Ll_1, m_k}^{Mm_1, l_k}$
2. form primitive Coulomb integrals $J_{ij}^{LM} = \sum_{kl} I_{ijkl}^L P_{kl}^{LM}$

3. form the full Coulomb matrix $J_{ij} = \sum_{ijLM} G_{Ll_i, m_j}^{Mm_i, l_j} J_{ij}^{LM}$

Step 2 above can be made computationally efficient by employing the factorization of the primitive integrals, reducing the scaling from N_p^4 to N_p^2 , as well as using matrix-vector products in the remaining N_p^4 step for contracting the non-factorizable intraelement integrals with the density matrix.

2.6.3 Exchange matrix

The exchange matrix is given by

$$K_{jk}^\sigma = \sum_{il} (ij|kl) P_{il}^\sigma, \quad (73)$$

which reduces to

$$K_{jk}^\sigma = \sum_{L_{\min}}^{L_{\max}} I_{ijkl}^L \left(P_{il}^\sigma G_{Ll_i, m_j}^{Mm_i, l_j} G_{Ll_l, m_k}^{Mm_l, l_k} \right). \quad (74)$$

As with the case of the Coulomb matrix above, it is beneficial to construct auxiliary density matrices by performing the sums over the angles in the first step, as this decreases the number of costly radial contractions. However, in the case of the exchange, the angular parts cannot be formed separately in the input and output indices, and so separate auxiliary density matrices need to be built for every block of the output jk .

The factorization of the interelement two-electron integrals can again be exploited in the radial contractions, reducing the scaling from N_p^4 to N_p^3 . The intraelement integrals are made more efficient by precomputing $i \leftrightarrow k$ permuted copies of the intraelement two-electron integrals and storing them in memory, which allows the use of efficient matrix-vector products for the contraction (N_p^4 cost).

2.7 Electric field

Although electrons are formally unbound in the presence of a finite field, in practice this is not a problem if the field is weak enough microscopically – macroscopically, such fields are still extremely strong. Placing the atom in an electric dipole field in the z direction changes the Hamiltonian by

$$\Delta H^{\text{dip}} = -\boldsymbol{\mu} \cdot \mathbf{E} = -\mu_z E_z = +z E_z \quad (75)$$

where the dipole matrix is given by

$$\mu_{z;ij} = 2\sqrt{\frac{\pi}{3}} G_{l_j 1, l_i}^{m_j 0, m_i} \int r B_i(r) B_j(r) dr \quad (76)$$

since

$$\mu_z = z = r \cos \theta, \quad (77)$$

$$\cos \theta = 2\sqrt{\frac{\pi}{3}} Y_1^0 = 2\sqrt{\frac{\pi}{3}} (Y_1^0)^*. \quad (78)$$

For a quadrupole field we have

$$\Delta H^{\text{quad}} = -\frac{1}{3}\Theta_{zz}E_{zz}, \quad (79)$$

where the quadrupole operator is

$$\Theta_{zz} = \frac{1}{2}(3z^2 - r^2) = (3\cos^2\theta - 1)r^2 \quad (80)$$

from which

$$\Theta_{zz;ij} = \frac{2}{5}\sqrt{5\pi}G_{l_j 2, l_i}^{m_j 0, m_i} \int r^2 B_i(r) B_j(r) dr. \quad (81)$$

2.8 Radial expectation values

Radial expectation values of the wave function can be obtained simply as

$$\langle r^n \rangle_{ij} = \delta_{l_i, l_j} \delta_{m_i, m_j} \int B_i(r) r^n B_j(r) dr. \quad (82)$$

2.9 Electron density at the nucleus

The inclusion of the r^{-1} factor in the basis makes it slightly non-trivial to calculate the electron density at the nucleus, as the electron density in the slice $[r, r + dr]$ is given by

$$\bar{n}(r) = \sum_{\mu\nu} \int P_{\mu\nu} \chi_{\mu}^*(\mathbf{r}) \chi_{\nu}(\mathbf{r}) d\Omega = \sqrt{4\pi} G_{0l_i, m_j}^{0m_i, l_j} \sum_{\mu\nu} P_{\mu\nu} \frac{B_{\mu}(r) B_{\nu}(r)}{r^2} \quad (83)$$

where at the nucleus both $B_n(r) \rightarrow 0$ and $r \rightarrow 0$. However, the electron density at the nucleus is straightforwardly obtained using two applications of l'Hôpital's rule as

$$n_0 = \bar{n}(0)/4\pi = \frac{1}{\sqrt{4\pi}} G_{0l_i, m_j}^{0m_i, l_j} \sum_{\mu\nu} P_{\mu\nu} B'_{\mu}(0) B'_{\nu}(0) \quad (84)$$

as $B_{\mu}(0) = 0$ due to the boundary conditions.

2.10 One-center expansions

Single-center expansions – in which the electronic structure of a polyatomic molecule is expanded in terms of functions on a single center – have been around in quantum chemistry for a long time.^{78–80} While the single-center method is not employed in the present work, for completeness we shall detail its use below, as it is also available in HELFEM for calculations on diatomics XY or linear triatomics XYX. An implementation of the single-center expansion for diatomic molecules based on B-splines has been published recently with applications to first- and second-period diatomics.⁸¹

As the orbitals in linear molecules can be classified by their m value, linear molecules are the most interesting use case for a one-center expansion, since the m component can be

treated analytically as for free atoms, while an expansion in l is necessary as the spherical symmetry of the system is broken by the off-center nuclear charges. Using the Laplace expansion for the Coulomb interaction (equation (47)) the nuclear attraction matrix elements for a nucleus at $z = a$ can be obtained as

$$V_{ij} = \left\langle i \left| -\frac{Z}{r_a} \right| j \right\rangle = -Z \int B_i(r) B_j(r) \frac{4\pi}{r_>} \sum_{L=0}^{\infty} \frac{1}{2L+1} \left(\frac{r_{<}}{r_>} \right)^L \times \sum_{M=-L}^L (Y_{l_i}^{m_i}(\Omega))^* Y_L^M(\Omega) (Y_L^M(\Omega_a))^* Y_{l_j}^{m_j}(\Omega) dr d\Omega \quad (85)$$

$$= -Z \int B_i(r) B_j(r) \frac{4\pi}{r_>} \sum_{L=0}^{\infty} \frac{1}{2L+1} \left(\frac{r_{<}}{r_>} \right)^L (Y_{l_i}^{m_i}(\Omega))^* Y_L^0(\Omega) (Y_L^0(\Omega_a))^* Y_{l_j}^{m_j}(\Omega) dr d\Omega. \quad (86)$$

This simplifies to

$$V_{ij} = -Z \int B_i(r) B_j(r) \frac{4\pi}{r_>} \sum_{L=0}^{\infty} \frac{1}{2L+1} \left(\frac{r_{<}}{r_>} \right)^L G_{Ll_j, m_i}^{0m_j, m_i} (Y_L^0(\Omega_a))^* dr \quad (87)$$

$$= -4\pi Z \sum_{L=0}^{\infty} \frac{1}{2L+1} G_{Ll_j, m_i}^{0m_j, l_i} \int B_i(r) B_j(r) \frac{1}{r_>} \left(\frac{r_{<}}{r_>} \right)^L \sqrt{\frac{2L+1}{4\pi}} P_L(\cos \theta_a) dr \quad (88)$$

$$= -Z \sum_{L=0}^{\infty} (\pm 1)^L \sqrt{\frac{4\pi}{2L+1}} G_{Ll_j, m_i}^{0m_j, l_i} \int B_i(r) B_j(r) \frac{1}{r_>} \left(\frac{r_{<}}{r_>} \right)^L dr \quad (89)$$

where we have used $P_L^0(\pm 1) = (\pm 1)^L$.

As with the two-electron integrals above, the integral splits into two cases, depending on the location of the element with respect to the off-center nuclear charge. From this splitting, it is apparent that element boundaries should be placed at the off-center nuclei, as this makes the implementation simpler, and allows for a better description of the nuclear cusp. A single radial grid is then no longer sufficient; due to the additional nucleus, the radial grid should first cover the region between the two nuclei $[0, a]$, and then the region from the additional nucleus to the practical infinity $[a, R_{\infty}]$, requiring that one converge the calculations with respect to both parts of the grid.

Further challenges of this approach are seen in equation (89): the various l channels couple together via L , and the couplings die off slowly. As the expansion in increasing l describes smaller and smaller features in the system – especially around the off-center nuclei – the single-center expansion works best for light systems with no tightly bound core orbitals. While the one-center approach could be used for molecules with more than two atoms, the restriction to linear molecules along with the difficulties describing heavy off-center atoms in effect limits one to the treatment of hydrides, either of the diatomic HX form, or the triatomic HXH form, where X is a heavy element. However, linear triatomic hydrides only occur in the alkaline series (BeH₂, MgH₂, ...), while arbitrary diatomic molecules can be treated efficiently using the prolate spheroidal coordinate system discussed in the second part of the series.⁵⁸ In the prolate spheroidal coordinate system the singularities at the nuclei vanish in the integration of the nuclear potential matrices, guaranteeing fast convergence to the CBS limit, at variance to the single-center expansion.

2.11 Density functional theory

The implementation of density functional theory in HELFEM is done exactly the same way as in our Gaussian-basis program, ERKALE.^{16,17} Given an expression for the exchange-correlation energy at the LGA, GGA or meta-GGA level

$$E_{xc} = \int f_{xc}(n_\alpha, n_\beta, \gamma_{\alpha\alpha}, \gamma_{\alpha\beta}, \gamma_{\beta\beta}, \tau_\alpha, \tau_\beta) d^3r, \quad (90)$$

where n_σ is the spin- σ density and the reduced gradient and kinetic energy density are given by

$$\gamma_{\sigma\sigma'} = \sqrt{\nabla n_\sigma \cdot \nabla n_{\sigma'}}, \quad (91)$$

$$\tau = \frac{1}{2} \sum_{i \text{ occ}} |\nabla \psi_i|^2, \quad (92)$$

respectively, the contribution to the Fock matrix is obtained as^{67,68}

$$K_{\mu\nu}^{xc;\sigma} = \int \left[\frac{\delta f_{xc}}{\delta n_\sigma(\mathbf{r})} \phi_\mu(\mathbf{r}) \phi_\nu(\mathbf{r}) + \frac{1}{2} \frac{\partial f_{xc}}{\partial \tau_\sigma} \nabla \chi_i \cdot \nabla \chi_j + \left(2 \frac{\delta f_{xc}}{\delta \gamma_{\sigma\sigma}(\mathbf{r})} \nabla n_\sigma(\mathbf{r}) + \frac{\delta f_{xc}}{\delta \gamma_{\sigma\sigma'}(\mathbf{r})} \nabla n_{\sigma'}(\mathbf{r}) \right) \cdot \nabla (\phi_\mu(\mathbf{r}) \phi_\nu(\mathbf{r})) \right] d^3r \quad (93)$$

The quadrature in equation (93) is formulated efficiently employing matrix-matrix products.

Due to the strict locality of the radial elements, it makes sense to do the integrals element by element, as the resulting Fock matrix is banded diagonal. Equation (93) contains three quadratures: one radial, and two angular (θ and ϕ). The same Gauss–Chebyshev radial quadrature is used for the radial part as for all the preceding matrix elements. However, the angular part is performed differently. Gauss–Chebyshev quadrature is used for the θ part, while a uniform grid is used for the ϕ part as it already yields exactness properties.⁸² Note that in contrast to the general molecular case, here the angular features of the electron density are more restricted due to the finite m expansion, and so the use of a compound rule such as Lebedev quadrature^{83,84} is less efficient. We have chosen $n_\theta = 4l_{\max} + 10$ and $n_\phi = 4m_{\max} + 5$ as the default values, which should guarantee sufficient accuracy for the quadrature even for meta-GGA functionals.

A noteworthy difference in the DFT implementation from the Cartesian case is that due to the curvilinear coordinate system, the dot products are computed differently as

$$\nabla f \cdot \nabla f = \sum_i \left(\frac{\hat{\mathbf{e}}_i \cdot \hat{\mathbf{e}}_i}{h_i^2} \left(\frac{\partial f}{\partial q_i} \right)^2 \right) = \sum_i \frac{1}{h_i^2} \left(\frac{\partial f}{\partial q_i} \right)^2 \quad (94)$$

where the scale factors for spherical polar coordinates are

$$h_r = 1, \quad (95)$$

$$h_\theta = r, \quad (96)$$

$$h_\phi = r \sin \theta. \quad (97)$$

In range-separated exchange functionals, the two-electron Coulomb operator $1/r_{12}$ is decomposed into a short-range and a long-range part as⁸⁵

$$\frac{1}{r_{12}} = \frac{\phi_{\text{sr}}(r_{12}; \omega)}{r_{12}} + \frac{1 - \phi_{\text{sr}}(r_{12}; \omega)}{r_{12}}, \quad (98)$$

where $\phi_{\text{sr}}(r_{12}; \omega)$ is a screening function and ω controls the speed of the screening. In almost all commonly used range-separated functionals, such as CAM-B3LYP;⁸⁶ the range-separated Minnesota functionals M11,⁸⁷ N12-SX,⁸⁸ and MN12-SX;⁸⁸ as well as the Head-Gordon group’s ω B97,⁸⁹ ω B97X,⁸⁹ ω B97X-V,⁹⁰ and ω B97M-V⁹¹ functionals, the weight function is chosen as

$$\phi_{\text{sr}}(r; \omega) = \text{erfc}(r; \omega), \quad (99)$$

as this choice is extremely convenient for implementation in programs employing Gaussian basis sets.^{92,93} The implementation of the range-separated functionals in the present approach would require the calculation of a Laplace expansion alike equation (47) for $\phi_{\text{sr}}(r_{12}; \omega)/r_{12}$, which is outside the scope of the present work.

3 Computational details

The equations presented above in section §2 have been implemented HELFEM in C++, employing the ARMADILLO library for linear algebra.^{94,95} Efficient basic linear algebra sub-routine (BLAS) libraries are used for the matrix operations with ARMADILLO. OPENMP parallelization is used throughout the program.

The one-electron and primitive two-electron integrals are computed once at the beginning of the calculation, and stored in memory. Radial integrals are evaluated with $5N_p$ points, which we have estimated to be sufficient even for the highly non-linear integrals in DFT, N_p being the number of shape functions per element. The memory requirements for the integrals are small, as instead of the full two-electron integral tensor, only the auxiliary integrals are stored. Furthermore, only the intraelement auxiliary integrals are stored as a rank-4 tensor, whereas the interelement integrals are stored in factorial form, which also allows for faster formation of the Coulomb and exchange matrices as was described above in the Theory section.

The LIBXC library⁹ is used to evaluate all exchange-correlation functionals. The core guess, *i.e.* eigenvectors of $\mathbf{H}_0 = \mathbf{T} + \mathbf{V}$ are used for initialization of the SCF calculations, and the Aufbau principle is employed to determine orbital occupations during the SCF cycle, unless the occupied orbital symmetries have been explicitly specified. Convergence of the SCF procedure is accelerated with a combination of the DIIS and ADIIS accelerators.¹³⁻¹⁵ Unless otherwise stated, the calculations have been converged to an orbital gradient *i.e.* DIIS error of 10^{-7} .

Calculations can be performed in HELFEM with fully spin-restricted orbitals, restricted open-shell orbitals via the constrained unrestricted HF update,^{96,97} or fully spin-unrestricted orbitals. The orbitals are updated by full diagonalization. Depending on the targeted orbital symmetry, the diagonalization can be performed in angular subblocks: by default, the diagonalization splits by m block, a symmetry which is maintained even under an electric field unless the orbitals break symmetry.

4 Results

4.1 Choice of element type and radial grid

To apply the new HELFEM program to calculations, we must first establish the best way to use it. As in the atomic case the angular basis is determined by the occupied orbital symmetries that are typically known in advance, the only remaining question is the radial basis. As FEM calculations can be converged to the basis set limit either by increasing the *number* of elements, or by increasing their *order*, the question is which approach yields the fastest convergence for a given number of basis functions. We shall first tackle the question of the radial grid, which has long been recognized as crucial to the efficiency of real-space approaches.⁹⁸ In contrast to finite-difference approaches that typically use a logarithmic radial coordinate,⁹⁹ the present implementation employs an untransformed r coordinate; thus, in analogy to previously published B-spline implementations,^{100,101} the optimal element spacing is probably not an uniform one.

Although adaptive approaches could be used to determine the most efficient element grid – see *e.g.* ref. 102 and refs. 62,63 for h -adaptive and p -adaptive approaches, respectively – it is evident that such an approach, while certainly possible, is not necessary given the high amount of symmetry present in the atomic problem. As the only problem is to determine a suitably accurate radial grid, and as atomic calculations are not computationally costly even with large grids, it suffices to just pick a grid large enough to yield a fully converged result. We will thus focus on universal optimizations of the element grid by global parametrizations of the placement of the elements in order to yield efficient grids for all atoms. The question is thus: what is the optimal way to arrange the elements?

The radial elements span the range $[0, r_\infty]$ where $r_\infty = 40a_0$ typically yields converged results, whereas larger values of r_∞ may be required for loosely bound anions.^{100,103} We have studied the problem by using N_{el} elements with uniform node spacing within the element, and varied the size distribution of the elements. The elements are defined by the placement of the borders between the elements, defined by the array r_i , with the i :th element ranging from r_i to r_{i+1} , with the numbering starting from 0. We have chosen to study four different types of element spacings:

1. a linear grid

$$r_i = \frac{i}{N} R_\infty \quad (100)$$

i.e. N uniform elements,

2. a quadratic grid

$$r_i = \frac{i^2}{N^2} R_\infty \quad (101)$$

which places leads to a denser grid near the nucleus and which has been previously suggested to be optimal for atoms,¹⁰⁴

3. a generalized polynomial grid

$$r_i = \frac{i^x}{N^x} R_\infty \quad (102)$$

i.e. a generalization of the linear and quadratic grids to arbitrary order, resulting in a denser grid near the nucleus for higher x values, where x is a constant defining the grid,

4. an exponential grid

$$r_i = (1 + R_\infty)^{ix/N^x} - 1 \quad (103)$$

which leads to even denser grids near the nucleus than the generalized polynomial grid above.

Note that x in equations (102) and (103) has nothing to do with the primitive coordinate system used in the quadrature in equations (41) to (45).

Because the generalized polynomial grid yields the linear and quadratic grids with $x = 1$ and $x = 2$, respectively, it suffices to study the performance of the generalized polynomial and exponential grids in the following. While a larger value of x results in more points in the energy-sensitive regions near the nucleus, it also results in less points *i.e.* a poorer description in the valence region, implying that x cannot be chosen arbitrarily large.

The radial element grid turns out to be sensitive to the type of the used elements (LIP, HIP, 2nd order HIP, *etc.*), necessitating separate grid analyses for each element type. Despite claims to the contrary,^{59,60} we have found LIPs to outperform HIPs by a wide margin. Choosing $r_\infty = 40a_0$, figure 3 shows scans for the optimal element grid for argon for calculations with six-node uniform LIP elements, three-node uniform HIP elements, and two-node 2nd order uniform HIP elements, all corresponding to the use of a fifth-order primitive expansion. Because the larger number of functions overlaid across elements in HIP calculations leads to a fewer number of basis functions than in LIP calculations, the number of elements for the HIP calculations have been adjusted so that the number of HIP and LIP functions match as closely as possible.

Figure 3 shows that the best result in the exponential grid is orders of magnitude better than the best result in the polynomial grids, which include the commonly used linear and quadratic element grids. This result holds regardless of the element type: for LIPs, for HIPs of the first order, and for HIPs of the second order. The results for other noble atoms are similar to figure 3 (not shown).

Interestingly enough, even though the HIP elements yield significantly better results than the LIP elements when a linear or an exponential element grid with $x = 1$ is employed, with the 2nd degree HIP outperforming the (1st degree) HIP, this ranking changes radically when the element grid is optimized. The HIPs have a sharp minimum around $x = 1$ with the exponential grid, whereas for LIPs the performance can be significantly improved by tuning the value of x with the exponential grid. The polynomial grid yields worse results for all three kinds of elements. Note that even though the LIP basis does not explicitly enforce continuity of the derivative

$$\phi'_i(r) = \sum_j \frac{1}{r_i - r_j} \prod_{k=0, k \neq i, k \neq j}^{n-1} \frac{r - r_k}{r_i - r_k}, \quad (104)$$

at the element boundaries in contrast to HIPs, this does not mean that the derivatives will be non-continuous across the boundary for LIPs. Namely, given the freedom of equation (104),

the variational principle will strive to make the derivative continuous across element boundaries even for LIPs, as a non-continuous derivative implies a higher kinetic energy.

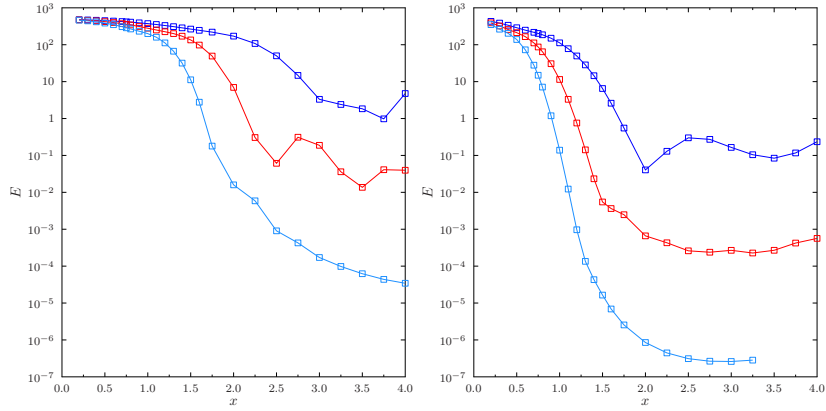
Having determined that LIPs are a better basis than HIPs, we continue by determining the optimal element grid. Employing $N = 5$, $N = 10$, $N = 20$, $N = 40$, $N = 80$, and $N = 160$ elements with 6-node uniform LIPs, we obtain the errors in the HF energies of the noble elements compared to literature values (ref. 103) shown in figures 4 to 10, with values of x ranging from 0.75 to 4.0 with a spacing of 0.25. Points not shown on the plots failed to converge to the used threshold, indicating the grid offers a poor description of the wave function.

As can be seen from the results, sublinear grids $x < 1$ yield poor results even for helium, while increasing the value of x dramatically improves the basis set. Even though the quadratic grid (polynomial with $x = 2$) is indeed better than the linear grid (polynomial with $x = 1$) as suggested in ref. 104, we find that much better results are obtained with the exponential grid (equation (103)), which is also less sensitive to the chosen value of x than the polynomial grid (equation (102)). Based on these results, we have chosen the default grid for atomic calculations to be the exponential one with $x = 2$, which appears to offer the best compromise between convergence and stability.

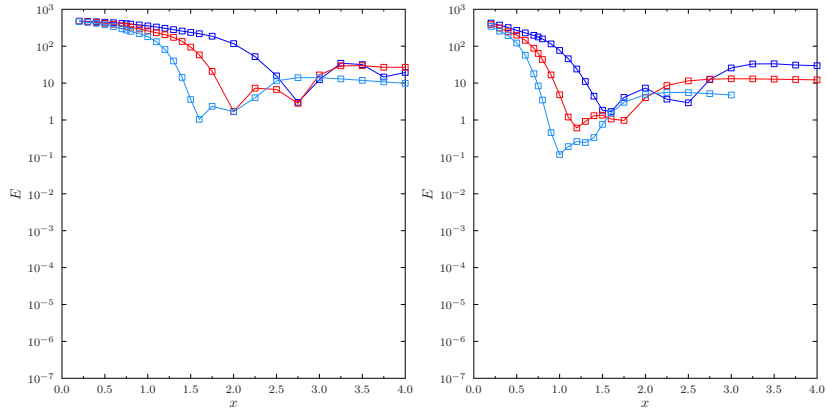
4.2 Choice of element order

The supremacy of LIPs is very convenient for calculations, as LIPs can be made numerically stable even at high orders, as was discussed above in the Theory section. We now proceed by studying the efficiency of LIPs with various numbers of nodes. For low numbers of nodes, the primitive expansion (equation (9)) with uniform node spacing, the analytical LIP expressions (equation (5)) with Lobatto node spacing, and Legendre polynomials (equations (10) to (12)) all yield similar results (not shown). For higher numbers of nodes, the primitive expansion is no longer numerically stable, but the Lobatto scheme and Legendre polynomials still yield similar results (not shown). Thus, we have chosen the Lobatto elements as the default, as they can be easily obtained, and employ them to study the speed of convergence to the basis set limit.

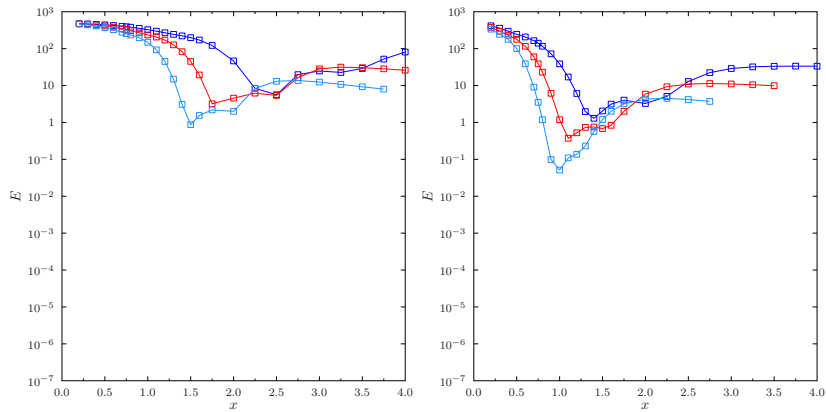
The calculations we will shortly present employ the exponential grid with $x = 2$, which was tuned above for 6-node uniform LIP elements. One might imagine that this choice of grid would be biased towards the 6-node elements, or that the use of the non-linear grid would favor using more elements with fewer nodes instead of fewer elements with more nodes. However, these speculations are emphatically rejected by the results shown in figure 11 for the errors in the total energy of the argon and krypton atoms: the use of high-order elements drastically improves convergence, yielding orders of magnitude more accuracy for the same number of basis functions. For example, while the energy for Ar is converged to the accuracy $O(10^{-9})$ of the reference result¹⁰³ with ~ 80 radial basis functions using 12-node LIPs, the similar-size calculation with 6-node LIPs only has an accuracy of $O(10^{-5})$. Although clearly the basis set limit can be reached with any of the primitive basis sets – provided enough elements – the higher order polynomials provide an astounding speedup



(a) Six-node LIP: 5 elements (blue), 10 elements (red), and 20 elements (cyan), yielding 24, 49, and 99 radial functions.



(b) Three-node HIP: 6 elements (blue), 12 elements (red), and 24 elements (cyan), yielding 23, 47, and 95 radial functions.



(c) Two-node 2nd order HIP: 8 elements (blue), 16 elements (red), and 32 elements (cyan), yielding 23, 47, and 95 radial functions.

Figure 3: Error in HF energy for argon with a polynomial (left) or exponential (right) grid, employing a different types of elements. The reference energy is $10^3 \cdot -526.817512803$.

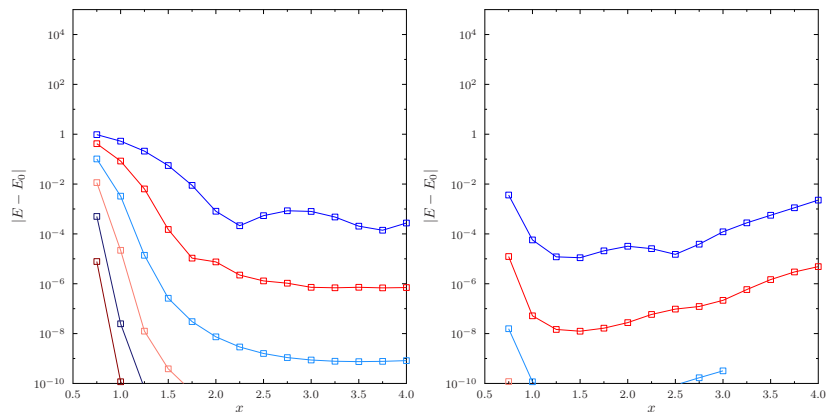


Figure 4: Error in HF energy for helium with a polynomial (left) or exponential (right) grid, employing 5 (blue), 10 (red), 20 (light blue), 40 (salmon), 80 (dark blue), or 160 elements (dark red) employing six-node uniform LIPs. The reference energy is $^{103} -2.8616799956$.

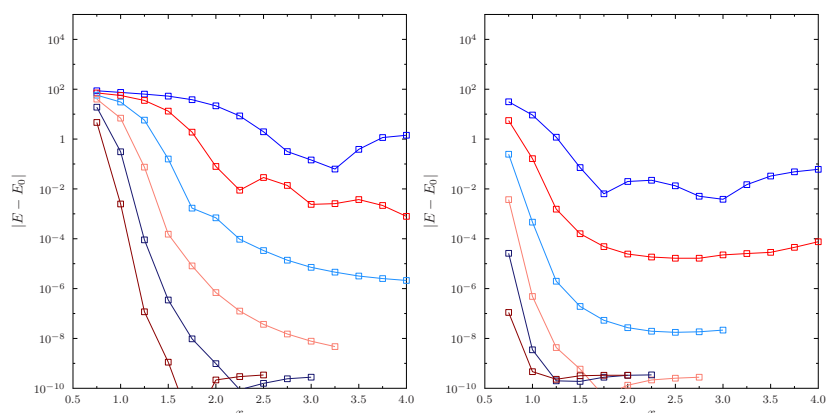


Figure 5: Error in HF energy for neon with a polynomial (left) or exponential (right) grid, employing 5 (blue), 10 (red), 20 (light blue), 40 (salmon), 80 (dark blue), or 160 elements (dark red) employing six-node uniform LIPs. The reference energy is $^{103} -128.547098109$.

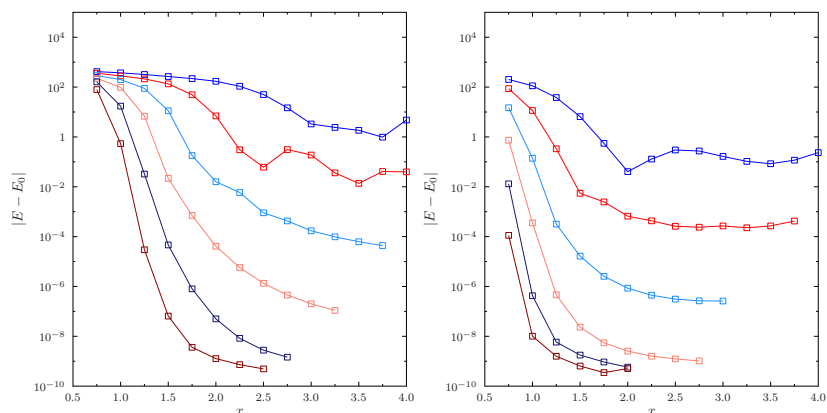


Figure 6: Error in HF energy for argon with a polynomial (left) or exponential (right) grid, employing 5 (blue), 10 (red), 20 (light blue), 40 (salmon), 80 (dark blue), or 160 elements (dark red) employing six-node uniform LIPs. The reference energy is $^{103} -526.817512803$.

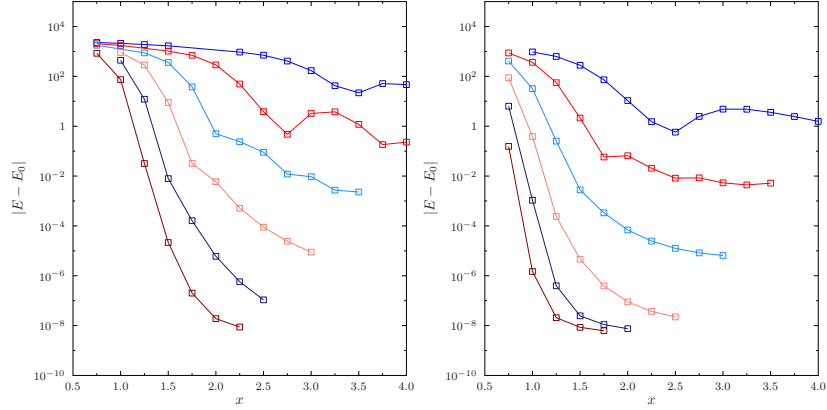


Figure 7: Error in HF energy for krypton with a polynomial (left) or exponential (right) grid, employing 5 (blue), 10 (red), 20 (light blue), 40 (salmon), 80 (dark blue), or 160 elements (dark red) employing six-node uniform LIPs. The reference energy is $^{103}\text{-}2752.05497735$.

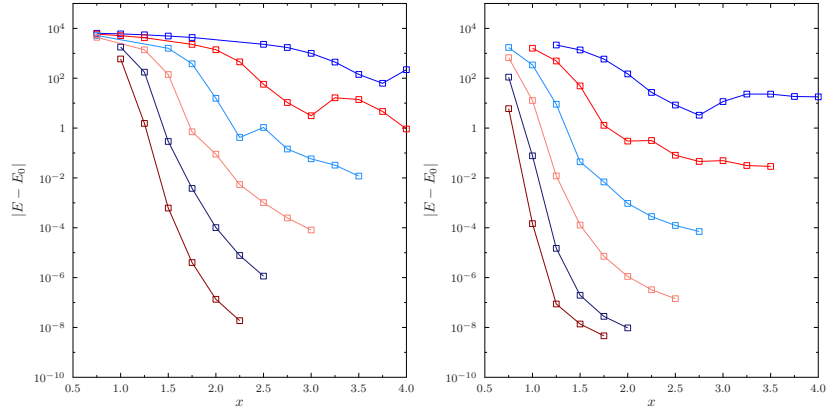


Figure 8: Error in HF energy for xenon with a polynomial (left) or exponential (right) grid, employing 5 (blue), 10 (red), 20 (light blue), 40 (salmon), 80 (dark blue), or 160 elements (dark red) employing six-node uniform LIPs. The reference energy is $^{103}\text{-}7232.13836387$.

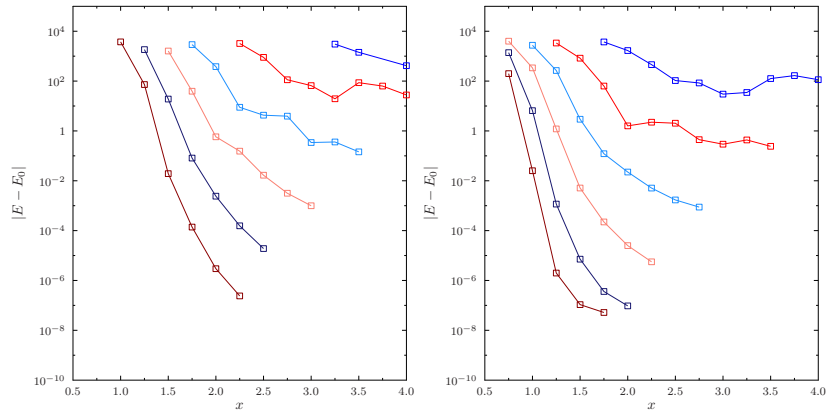


Figure 9: Error in HF energy for radon with a polynomial (left) or exponential (right) grid, employing 5 (blue), 10 (red), 20 (light blue), 40 (salmon), 80 (dark blue), or 160 elements (dark red) employing six-node uniform LIPs. The reference energy is $^{103}\text{-}21866.7722409$.

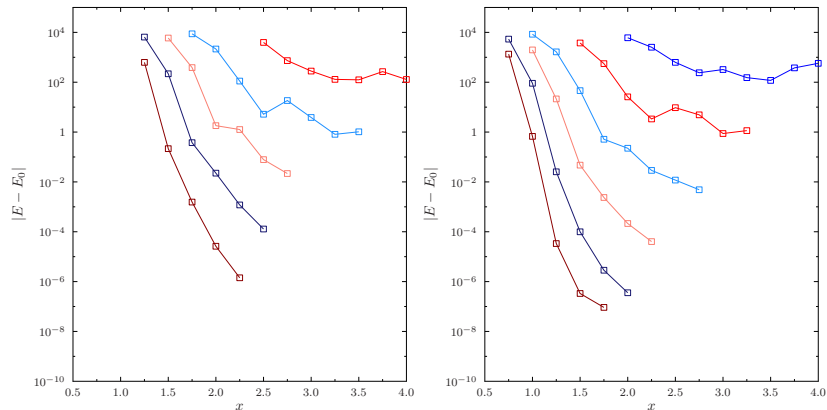


Figure 10: Error in HF energy for oganesson with a polynomial (left) or exponential (right) grid, employing 5 (blue), 10 (red), 20 (light blue), 40 (salmon), 80 (dark blue), or 160 elements (dark red) employing six-node uniform LIPs. The reference energy is $^{103}\text{-}46324.3558151$.

in convergence. Similar results have been obtained recently for three-dimensional meshes in molecular calculations.¹⁰⁵

The drawback of the high-order elements is not only that higher-order quadrature rules are needed, but also that the storage costs of the primitive two-electron integrals is increased. However, based on the amazing accuracy benefits of higher-order polynomials, we have chosen 15-node LIPs as the default in HELFEM, which are also used for the rest of the manuscript.

4.3 Electric response

We demonstrate the code with electric response calculations on Li^+ and Sr^{2+} for which HF benchmark values are available in ref. 41. As the perturbation caused by the electric field is most strongly felt by the valence orbitals, accurate calculation of the electric response requires a fine representation of the valence region, whereas the core orbitals are mostly unaffected. Since the radial grid we have chosen emphasizes the core region over the valence region, a large number of elements may be necessary to converge the electric properties. It is possible that more accurate electric properties could be reproduced by re-evaluating the emphases of the radial grid by sacrificing accuracy in the inert core region for more flexibility in the valence region. However, as we wish to reproduce both the absolute energies and electric properties exactly for comparison with ref. 41, a large radial grid with 10 elements *i.e.* 139 radial functions will be used. For these calculations we set $r_\infty = 40a_0$, and an orbital gradient convergence threshold of 10^{-8} . In this radial grid, the atomic energies are converged to beyond nanohartree accuracy, as can be verified by doubling the number of elements (not shown).

Because the dipole field has a l component (see equations (75), (77) and (78)), it generates higher l components in an atomic wave function that would otherwise lack them. In order to calculate, for instance, static dipole polarizabilities with the present approach, it is first necessary to determine how well the expansion converges. Because the field was chosen to be weak, using numerical values determined in ref. 41, the response of the wave function should be linear, and that of the energy quadratic.

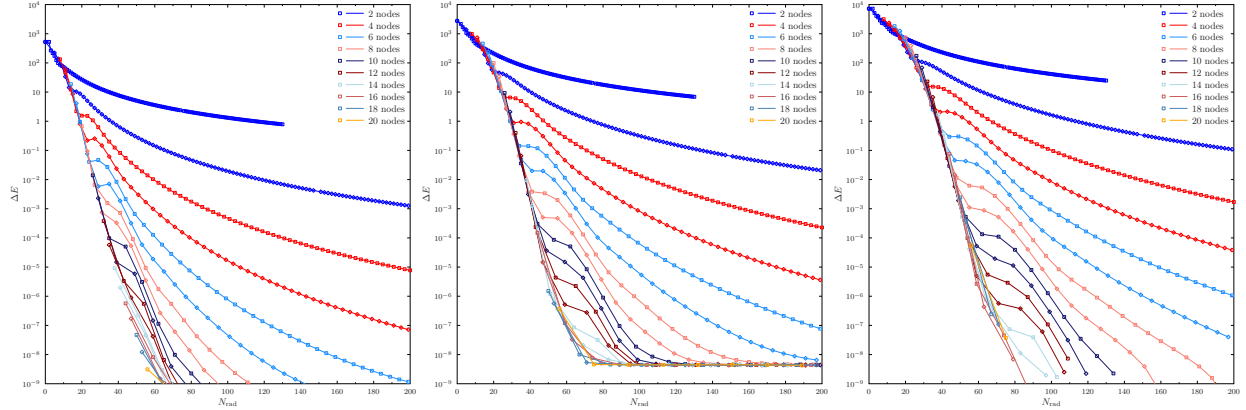


Figure 11: Error in HF energy for argon, krypton, and xenon as function of size of radial basis set with LIP elements employing 2 to 20 Lobatto nodes. The legend shows the colors for even numbers of nodes (square markers), whereas the consecutive odd-number node result is shown in the same color with diamond markers. The topmost two curves correspond to 2 and 3 node elements, correspondingly.

It is instructive to begin the analysis from Li^+ , as its electronic configuration at zero field is simply $1s^2$. The values for the energy, dipole moment and quadrupole moment of Li^+ for increasing sizes of the basis set are given in table 1. No angular freedom exists in the atomic basis set consisting only of Y_0^0 , and so the energy is constant and the dipole and quadrupole moments vanish for $l_{\max} = 0$. Adding the first polarization shell decreases the energy at finite fields noticeably, but the energy appears already to have reached converge. In contrast, the dipole and quadrupole moments change noticeably upon the addition of a second polarization shell, as well. While the effect is small for the dipole moment, for the quadrupole moment the first and second polarization shells appear to be of equal importance. The addition of a third polarization shell appears insignificant.

Next, we move on to Sr^{2+} , which has the electronic configuration $1s^2 2s^2 2p^6 3s^2 3p^6 4s^2 3d^{10} 4p^6$, and the values for the energy, dipole moment and quadrupole moment for increasing sizes of the basis set are given in table 2. Based on the experience with Li^+ above, as the atomic basis set already contains full flexibility for polarizing the ns levels, partial flexibility for polarizing the np levels, but no flexibility for the $3d$ level, it can be assumed that the results should be close to converged with the atomic basis set, as the $3d$ orbitals are considerably more bound ($\epsilon = -6.1856E_h$) than the $4s$ ($\epsilon = -2.3755E_h$) or $4p$ ($\epsilon = -1.5786$) levels. Indeed, it can be seen that in addition to the energy, also the dipole and quadrupole moments converge to numerical precision (with the used field strengths) with a single additional polarization shell in this case. Having established that the results for Li^+ and Sr^{2+} are converged with $l_{\max} = 2$ and $l_{\max} = 3$, respectively, we can proceed by comparison of the field-dependent energy, dipole moment and quadrupole moment against literature data from ref. 41. These results are shown in table 3.

In the case of Li^+ , the energies are in perfect agreement for the 11 first decimals. For the dipole moments, discrepancies can be seen in the sixth decimal, meaning that the first six digits are converged, while the quadrupole moment appears to carry a five-digit accuracy, with discrepancies seen in the fourth decimal.

There is a constant 7 nanohartree difference Sr^{2+} at all values of the finite field, with the value of ref. 41 undercutting the value obtained in the present work. As stated above, we have checked that our basis is accurate at least to nanohartree level. However, contrary to the present work, the approach used in ref. 41 is non-variational. The relative error estimated for the total energy of the Sr^{2+} calculation in ref. 41 was 2×10^{-13} , which translates to $0.6 \text{ n}E_h$, ten times less than the observed difference. Still, we are fairly confident that this is the reason for the discrepancy between the results.

Differences between the dipole moments of Sr^{2+} can be seen in the fifth decimal, whereas differences in the quadrupole moment appear already at the third decimal for the largest field. Overall, the agreement is clearly satisfactory, while we again note that for accurate applications of the present methodology to electric properties, the choice of the radial grid could be investigated in more detail.

Next, static dipole polarizabilities

$$\alpha_{zz} = \left(\frac{d\mu_z}{dE_z} \right)_{E_z=0} \quad (105)$$

can be extracted from the data at finite fields given in table 3 by employing finite difference approximations such as the two-point rule

$$f'(x) \approx \frac{f(x+h) - f(x-h)}{2h} + O(h^2) \quad (106)$$

or the four-point rule

$$f'(x) \approx \frac{-f(x+2h) + 8f(x+h) - 8f(x-h) + f(x-2h)}{12h} + O(h^4); \quad (107)$$

these results are shown in table 4. The values for the polarizability in table 4 have been obtained with equation (107), whereas the error estimate is simply the difference between the four-point and two-point values given by equations (107) and (106), respectively. The HF polarizability agrees well with literature values from ref. 41, which are $1.89474455 \times 10^{-1}$ for Li^+ (discrepance at sixth decimal) and 5.8843416 for Sr^{2+} (full agreement). Table 4 also presents analogous calculations at various levels of DFT with the LDA,⁴²⁻⁴⁴ PBE^{45,46} and TPSS^{49,50} functionals, and their hybrids; PBEh^{47,48} and TPSSH,⁵¹ respectively. All DFT functionals predict a higher polarizability, *i.e.* a more flexible electron density than the one reproduced by HF.

4.4 Accuracy of Gaussian basis sets

In order to study the accuracy of the results obtained with an extended Gaussian basis set in ref. 56, we decided to repeat the calculations in the finite element approach. We chose to study the species H^- , He, Li^+ , Li^- , Be, B^+ , C^- , N, O^+ , F^- , Ne, Na^+ , Na^- , Mg, Al^+ , Si^- , P, S^+ , Cl^- , and Ar, as each of them has only fully filled subshells.

Although systems with partially filled shells can also be computed with the present approach, the corresponding minimal-energy solutions are well-known to break symmetry unless spherical averaging is employed. Thus, instead of the expected exactness of the SCF

E_z	$l_{\max} = 0$	$l_{\max} = 1$	$l_{\max} = 2$	$l_{\max} = 3$	$l_{\max} = 4$
-0.006	-7.236415201	-3.41 (-6)	-6.63 (-12)	2.52 (-13)	1.27 (-13)
-0.004	-7.236415201	-1.52 (-6)	-2.12 (-13)	-6.42 (-13)	-7.90 (-14)
-0.002	-7.236415201	-3.79 (-7)	-3.20 (-14)	2.07 (-13)	-9.50 (-14)
0.000	-7.236415201	3.55 (-13)	2.42 (-13)	-3.45 (-13)	4.34 (-13)
0.002	-7.236415201	-3.79 (-7)	-3.20 (-14)	2.07 (-13)	-9.50 (-14)
0.004	-7.236415201	-1.52 (-6)	-2.12 (-13)	-6.42 (-13)	-7.90 (-14)
0.006	-7.236415201	-3.41 (-6)	-6.63 (-12)	2.52 (-13)	1.27 (-13)

(a) Energy

E_z	$l_{\max} = 0$	$l_{\max} = 1$	$l_{\max} = 2$	$l_{\max} = 3$	$l_{\max} = 4$
-0.006	0.00 (0)	1.14 (-3)	4.34 (-9)	3.62 (-14)	-4.15 (-13)
-0.004	0.00 (0)	7.58 (-4)	1.28 (-9)	-1.57 (-14)	1.52 (-14)
-0.002	0.00 (0)	3.79 (-4)	1.61 (-10)	4.95 (-15)	-1.82 (-14)
0.000	0.00 (0)	0.00 (0)	0.00 (0)	0.00 (0)	0.00 (0)
0.002	0.00 (0)	-3.79 (-4)	-1.61 (-10)	-4.95 (-15)	1.82 (-14)
0.004	0.00 (0)	-7.58 (-4)	-1.28 (-9)	1.57 (-14)	-1.52 (-14)
0.006	0.00 (0)	-1.14 (-3)	-4.34 (-9)	-3.62 (-14)	4.15 (-13)

(b) Dipole moment

E_z	$l_{\max} = 0$	$l_{\max} = 1$	$l_{\max} = 2$	$l_{\max} = 3$	$l_{\max} = 4$
-0.006	0.00 (0)	9.36 (-7)	1.17 (-6)	9.40 (-12)	-3.97 (-14)
-0.004	0.00 (0)	4.16 (-7)	5.18 (-7)	1.52 (-12)	-4.31 (-16)
-0.002	0.00 (0)	1.04 (-7)	1.30 (-7)	-3.29 (-14)	-5.74 (-14)
0.000	0.00 (0)	0.00 (0)	0.00 (0)	0.00 (0)	0.00 (0)
0.002	0.00 (0)	1.04 (-7)	1.30 (-7)	-3.29 (-14)	-5.74 (-14)
0.004	0.00 (0)	4.16 (-7)	5.18 (-7)	1.52 (-12)	-4.31 (-16)
0.006	0.00 (0)	9.36 (-7)	1.17 (-6)	9.40 (-12)	-3.97 (-14)

(c) Quadrupole moment

Table 1: Convergence of the electric properties of Li^+ in a finite field HF calculation. The first column lists the field strength, the second column gives the value of the property in the unmodified basis set for the atom with minimal l value, while the successive columns describe the change of the property from the previous l value. The values in the parentheses indicate magnitude, $A(n) = A \times 10^n$.

E_z	$l_{\max} = 2$	$l_{\max} = 3$	$l_{\max} = 4$	$l_{\max} = 5$	$l_{\max} = 6$
-0.0018	-3130.995692183	-1.08 (-8)	-3.64 (-12)	-7.14 (-11)	6.37 (-11)
-0.0012	-3130.995686893	-4.85 (-9)	4.55 (-11)	-9.64 (-11)	8.55 (-11)
-0.0006	-3130.995683719	-1.10 (-9)	-3.77 (-11)	-7.73 (-12)	3.91 (-11)
0.0000	-3130.995682661	2.46 (-11)	-4.32 (-11)	6.18 (-11)	-1.96 (-11)
0.0006	-3130.995683719	-1.10 (-9)	-3.77 (-11)	-7.73 (-12)	3.91 (-11)
0.0012	-3130.995686893	-4.85 (-9)	4.55 (-11)	-9.64 (-11)	8.55 (-11)
0.0018	-3130.995692183	-1.08 (-8)	-3.64 (-12)	-7.14 (-11)	6.37 (-11)

(a) Energy

E_z	$l_{\max} = 2$	$l_{\max} = 3$	$l_{\max} = 4$	$l_{\max} = 5$	$l_{\max} = 6$
-0.0018	1.06 (-2)	1.21 (-5)	-8.32 (-11)	1.50 (-11)	3.71 (-12)
-0.0012	7.05 (-3)	8.05 (-6)	1.54 (-10)	9.81 (-12)	1.23 (-11)
-0.0006	3.53 (-3)	4.02 (-6)	-2.73 (-11)	1.13 (-11)	-3.43 (-11)
0.0000	-3.11 (-9)	5.31 (-9)	-2.75 (-9)	-2.16 (-8)	5.37 (-9)
0.0006	-3.53 (-3)	-4.02 (-6)	2.73 (-11)	-1.13 (-11)	3.43 (-11)
0.0012	-7.05 (-3)	-8.05 (-6)	-1.54 (-10)	-9.81 (-12)	-1.23 (-11)
0.0018	-1.06 (-2)	-1.21 (-5)	8.32 (-11)	-1.50 (-11)	-3.71 (-12)

(b) Dipole moment

E_z	$l_{\max} = 2$	$l_{\max} = 3$	$l_{\max} = 4$	$l_{\max} = 5$	$l_{\max} = 6$
-0.0018	2.00 (-5)	1.49 (-5)	5.45 (-9)	1.12 (-10)	-5.96 (-11)
-0.0012	8.90 (-6)	6.61 (-6)	2.48 (-9)	-2.51 (-11)	3.91 (-11)
-0.0006	2.23 (-6)	1.65 (-6)	6.28 (-10)	1.38 (-11)	-5.41 (-11)
0.0000	4.52 (-10)	2.97 (-9)	-4.98 (-9)	-1.37 (-9)	7.39 (-9)
0.0006	2.23 (-6)	1.65 (-6)	6.28 (-10)	1.38 (-11)	-5.41 (-11)
0.0012	8.90 (-6)	6.61 (-6)	2.48 (-9)	-2.51 (-11)	3.91 (-11)
0.0018	2.00 (-5)	1.49 (-5)	5.45 (-9)	1.12 (-10)	-5.96 (-11)

(c) Quadrupole moment

Table 2: Convergence of the electric properties of Sr^{2+} in a finite field HF calculation. The notation is the same as in table 1.

E_z	present work			Literature value		
	Energy	Dipole	Quadrupole	Energy	Dipole	Quadrupole
-0.004	-7.23641671725	-7.578993 (-4)	-9.341741 (-7)	-7.23641671725	-7.579002 (-4)	-9.341812 (-7)
-0.002	-7.23641558040	-3.789487 (-4)	-2.335419 (-7)	-7.23641558040	-3.789492 (-4)	-2.335434 (-7)
0.000	-7.23641520145	0.0	0.0	-7.23641520145	-1.393330 (-14)	-5.228457 (-15)
0.002	-7.23641558040	3.789487 (-4)	-2.335419 (-7)	-7.23641558040	3.789492 (-4)	-2.335434 (-7)
0.004	-7.23641671725	7.578993 (-4)	-9.341741 (-7)	-7.23641671725	7.579002 (-4)	-9.341812 (-7)

(a) Li^+

E_z	present work			Literature value		
	Energy	Dipole	Quadrupole	Energy	Dipole	Quadrupole
-0.0012	-3130.995686898	-7.061234 (-3)	-1.550859 (-5)	-3130.995686905	-7.061227 (-3)	-1.551909 (-5)
-0.0006	-3130.995683720	-3.530623 (-3)	-3.866475 (-6)	-3130.995683727	-3.530607 (-3)	-3.879769 (-6)
0.0000	-3130.995682661	3.875110 (-9)	5.749758 (-9)	-3130.995682668	-9.387699 (-11)	-2.648433 (-11)
0.0006	-3130.995683720	3.530623 (-3)	-3.866475 (-6)	-3130.995683727	3.530607 (-3)	-3.879762 (-6)
0.0012	-3130.995686898	7.061234 (-3)	-1.550859 (-5)	-3130.995686905	7.061227 (-3)	-1.551909 (-5)

(b) Sr^{2+}

Table 3: Electric properties of Li^+ and Sr^{2+} in a finite field, compared to literature values from ref. 41 with a truncated number of decimals. The values in the parentheses indicate magnitude, $A(n) = A \times 10^n$.

method	$\mu_z, E_z = -2h$	$\mu_z, E_z = -h$	$\mu_z, E_z = 0$	$\mu_z, E_z = h$	$\mu_z, E_z = 2h$	α_{zz}	$\Delta\alpha_{zz}$
HF	-7.578993 (-4)	-3.789487 (-4)	0.000000 (0)	3.789487 (-4)	7.578993 (-4)	1.894742 (-1)	-1.52 (-7)
LDA	-8.602004 (-4)	-4.300989 (-4)	1.058460 (-16)	4.300989 (-4)	8.602004 (-4)	2.150492 (-1)	-2.21 (-7)
PBE	-8.317930 (-4)	-4.158951 (-4)	1.433630 (-15)	4.158951 (-4)	8.317930 (-4)	2.079473 (-1)	-2.25 (-7)
TPSS	-8.110240 (-4)	-4.055108 (-4)	1.139966 (-14)	4.055108 (-4)	8.110240 (-4)	2.027552 (-1)	-2.05 (-7)
PBEh	-8.096724 (-4)	-4.048350 (-4)	-6.712163 (-15)	4.048350 (-4)	8.096724 (-4)	2.024173 (-1)	-2.00 (-7)
TPSSh	-8.045716 (-4)	-4.022846 (-4)	9.588448 (-15)	4.022846 (-4)	8.045716 (-4)	2.011421 (-1)	-1.98 (-7)

(a) Li^+ , $h = 0.002$

method	$\mu_z, E_z = -2h$	$\mu_z, E_z = -h$	$\mu_z, E_z = 0$	$\mu_z, E_z = h$	$\mu_z, E_z = 2h$	α_{zz}	$\Delta\alpha_{zz}$
HF	-7.061227 (-3)	-3.530607 (-3)	-2.195314 (-9)	3.530607 (-3)	7.061227 (-3)	5.884342 (0)	-3.55 (-6)
LDA	-7.197242 (-3)	-3.598471 (-3)	9.338964 (-9)	3.598472 (-3)	7.197242 (-3)	5.997369 (0)	-8.30 (-5)
PBE	-7.218082 (-3)	-3.608891 (-3)	-4.167875 (-10)	3.608890 (-3)	7.218082 (-3)	6.014734 (0)	-8.37 (-5)
TPSS	-7.148780 (-3)	-3.574260 (-3)	-1.918774 (-8)	3.574260 (-3)	7.148779 (-3)	5.957027 (0)	-7.22 (-5)
PBEh	-7.136971 (-3)	-3.568168 (-3)	-1.432482 (-10)	3.568168 (-3)	7.136970 (-3)	5.946771 (0)	-1.76 (-4)
TPSSh	-7.123533 (-3)	-3.561625 (-3)	-7.538647 (-10)	3.561622 (-3)	7.123535 (-3)	5.935959 (0)	-7.97 (-5)

(b) Sr^{2+} , $h = 0.0006$

Table 4: Dipole moments μ_z at finite fields E_z , and the extracted dipole polarizabilities α_{zz} and its estimated error $\Delta\alpha_{zz}$ for Li^+ and Sr^{2+} at HF, LDA, PBE, TPSS, PBEh, and TPSSh levels of theory.

solution for second-period atoms with $l_{\max} = 1$, the energy is lowered by the addition of functions with higher l ; see for instance the discussion by Löwdin in ref. 106. In these cases, finding the lowest solution within the FEM approach may be nontrivial, as convergence may occur to any number of solutions. Surprisingly, symmetry breaking can sometimes also be seen for cases with fully filled shells, such as in the case of the Ne atom and the F^- anion.¹⁰⁷ We chose the above systems for the present work, as the study by Anderson and coworkers in ref. 56 explicitly considered broken symmetry solutions by the use of wave function stability analysis,^{108,109} which is not currently implemented in HELFEM.

Starting with HF, in agreement with ref. 100 we find that although the neutral atoms are converged with $r_\infty = 40a_0$, the extended anions Li^- and Na^- require a larger value to be employed. Whereas ref. 100 employed $r_\infty = 60a_0$, we chose $r_\infty = 80a_0$ as this changes the nanohartree digit of the energy of Na^- . Unlike ref. 56, the symmetries of the occupied orbitals were enforced, as this was found to speed up the convergence of the SCF procedure. The energies were found to converge to nanohartree accuracy with 10 radial elements.

The results for the HF calculations are shown in table 5. For further reference, we have repeated the aug-pc- ∞ Gaussian-basis calculations of ref. 56 with ERKALE; these results are also given in table 5. Tight integral screening thresholds were used in ERKALE. For comparison, table 5 also reports the energies given in the supplementary information of ref. 56. The aug-pc- ∞ basis of ref. 56 was originally developed by Jensen in ref. 55.

The HELFEM and ERKALE data are in excellent agreement: the FEM calculations yield energies that are up to a few dozen microhartree lower than the ones reproduced by the large Gaussian basis set. The agreement between the calculations performed in the present work and those of ref. 56 is also in general excellent, with three notable exceptions: the extended, weakly bound anions Li^- and Na^- , as well as the Be atom. In these cases, the energies reported in ref. 56 are considerably lower than the energies we have computed using FEM or with ERKALE using the same basis set as ref. 56. Comparison to literature values^{100,110,111} for these systems affirm the accuracy of the values produced in the present work. Our FEM values for the Li^- , Be, and Na^- are in perfect agreement with the literature values^{100,110,111} -7.428232061, -14.57302317, and -161.8551260, respectively, with the Gaussian basis values being consistently upper bounds to the converged values. We can thus conclude that the values reported in ref. 56 for Li^- , Be, and Na^- represent symmetry broken solutions of closed-shell species that have been discussed in ref. 107.

Repeating the calculations with the BHLYP functional,¹⁰ the results in table 6 are obtained. A (250,770) integration grid was employed in the ERKALE calculations, again with tight integral screening thresholds. The BHLYP functional binds Li^- and Na^- less strongly than HF, and the values for these systems profit from the chosen large value for r_∞ . Although the reported finite element energies for Li^- and Na^- are still in error by tens of nanohartrees compared to a larger value of r_∞ , the conclusions of our study are not affected. Namely, the HELFEM and ERKALE calculations are in excellent agreement, the differences between the two approaches being again in the microhartrees but somewhat smaller than in the case of the HF calculations in table 5.

As in the HF calculations, while the agreement with the results of ref. 56 is generally excellent, also here the values for Li^- and Na^- stand out, undercutting the converged complete basis set energy in the millihartree range. At variance to table 5, the energy for Be is now in perfect agreement. Instead, the energy for H^- of ref. 56 is too low by 1.6 mE_h , which

	finite element	Gaussian, ERKALE	Gaussian, ref. 56	difference (μE_h)
H ⁻	-0.487929734	-0.487929397	-0.48793	-0.34
He	-2.861679996	-2.861675168	-2.86168	-4.83
Li ⁺	-7.236415201	-7.236414275	-7.23641	-0.93
Li ⁻	-7.428232061	-7.428231023	-7.43152	-1.04
Be	-14.573023168	-14.573021658	-14.57335	-1.51
B ⁺	-24.237575184	-24.237566607	-24.23757	-8.58
C ⁻	-37.710309470	-37.710305344	-37.71031	-4.13
N	-54.404548303	-54.404543006	-54.40454	-5.30
O ⁺	-74.377133274	-74.377123988	-74.37712	-9.29
F ⁻	-99.459453913	-99.459442803	-99.45944	-11.11
Ne	-128.547098109	-128.547079874	-128.54708	-18.24
Na ⁺	-161.676962614	-161.676950741	-161.67695	-11.87
Na ⁻	-161.855125996	-161.855114256	-161.85702	-11.74
Mg	-199.614636424	-199.614623656	-199.61462	-12.77
Al ⁺	-241.674670465	-241.674657663	-241.67466	-12.80
Si ⁻	-288.890058853	-288.890044560	-288.89004	-14.29
P	-340.719275268	-340.719259261	-340.71926	-16.01
S ⁺	-397.173947455	-397.173928130	-397.17393	-19.33
Cl ⁻	-459.576925268	-459.576907117	-459.57691	-18.15
Ar	-526.817512803	-526.817490166	-526.81749	-22.64

Table 5: HF energies from a finite element calculation (present work, second column) compared to a Gaussian basis calculation with ERKALE using the basis set from ref. 56 (present work, third column). The fourth column shows the Gaussian basis set energies from ref. 56. The fifth column lists the energy difference between finite element and Gaussian basis set calculations of the present work in microhartree.

is again likely caused by symmetry breaking.

5 Summary and Conclusions

We have described the implementation of a finite element program called HELFEM⁸ for electronic structure calculations on atoms in the framework of Hartree–Fock (HF) or Kohn–Sham density functional theory. HELFEM is interfaced with the LIBXC library of exchange–correlation functionals,⁹ and supports calculations at the local spin-density approximation (LDA), generalized gradient approximation (GGA) and meta-GGA levels of theory, including hybrid functionals. Calculations can be performed with fully spin-restricted, spin-restricted open-shell, and spin-unrestricted orbitals.

We have suggested an exponential radial grid for atomic calculations that we have extensively tested in applications of the program on noble elements. The exponential grid with $x = 2$ was found to yield faster convergence to the basis set limit than commonly used linear or quadratic element grids.

Tests of the various kinds of elements supported by the program showed that Lagrange

	finite element	Gaussian, ERKALE	Gaussian, ref. 56	difference (μE_h)
H ⁻	-0.523455900	N/C	-0.52501	N/C
He	-2.905757890	-2.905754694	-2.90575	-3.20
Li ⁺	-7.281288205	-7.281287221	-7.28129	-0.98
Li ⁻	-7.500010377 ^a	N/C	-7.50081	N/C
Be	-14.664037985	-14.664035679	-14.66404	-2.31
B ⁺	-24.339819186	-24.339811410	-24.33981	-7.78
C ⁻	-37.887327417	-37.887323754	-37.88732	-3.66
N	-54.593153473	-54.593148512	-54.59315	-4.96
O ⁺	-74.575815265	-74.575805610	-74.57581	-9.66
F ⁻	-99.856395949	-99.856387120	-99.85639	-8.83
Ne	-128.948416397	-128.948403201	-128.94840	-13.20
Na ⁺	-162.083275414	-162.083265318	-162.08327	-10.10
Na ⁻	-162.293938337 ^a	N/C	-162.29465	N/C
Mg	-200.080754856	-200.080744137	-200.08074	-10.72
Al ⁺	-242.159244333	-242.159234002	-242.15923	-10.33
Si ⁻	-289.428472604	-289.428460403	-289.42846	-12.20
P	-341.278950750	-341.278937694	-341.27894	-13.06
S ⁺	-397.752619769	-397.752604276	-397.75260	-15.49
Cl ⁻	-460.295948313	-460.295933897	-460.29593	-14.42
Ar	-527.556251384	-527.556235529	-527.55624	-15.85

Table 6: BHLYP energies from a finite element calculation (present work) compared to a previously reported Gaussian basis calculation (ref. 56). Cases where the ERKALE calculations failed to converge are marked with N/C.

^aThe energy still changed by $-1.6 \times 10^{-7} E_h$ going from $R_\infty = 60a_0$ to $R_\infty = 80a_0$ (used value), and would lower $\sim 5 \times 10^{-8} E_h$ more by going from $R_\infty = 80a_0$ to $R_\infty = 100a_0$.

interpolating polynomials (LIPs) or Legendre polynomials outperform Hermite interpolating polynomials by a wide margin, and the use of high-order Lagrange/Legendre polynomials yields the most accurate results. 15-node LIPs with Lobatto nodes were chosen as the default radial basis in HELFEM.

The capabilities of the program were demonstrated by calculations of Li^+ and Sr^{2+} in an electric field, with the results at the HF limit being in good agreement with literature values.⁴¹ Furthermore, static dipole polarizabilities for Li^+ and Sr^{2+} were reported with the LDA, PBE, PBEh, TPSS, and TPSSh functionals.

Finally, the program was used to study the accuracy of recently reported atomic HF and DFT calculations employing Gaussian basis sets.⁵⁶ Cross-comparisons with results from the ERKALE program^{16,17} showed that the errors in the Gaussian basis set are only up to a few dozen microhartrees. Closed-shell symmetry-breaking effects were identified in the calculations of ref. 56, with energy lowerings of several millihartrees.

Funding information

This work has been supported by the Academy of Finland through project number 311149.

Acknowledgments

I thank Dage Sundholm and Gregory Beylkin for discussions, and Dage Sundholm and Pekka Pyykkö for comments on the manuscript. Computational resources provided by CSC – It Center for Science Ltd (Espoo, Finland) and the Finnish Grid and Cloud Infrastructure (persistent identifier urn:nbn:fi:research-infras-2016072533) are gratefully acknowledged.

References

- [1] P. Hohenberg and W. Kohn, Phys. Rev. **136**, B864 (1964), ISSN 0031-899X, URL <http://link.aps.org/doi/10.1103/PhysRev.136.B864>.
- [2] W. Kohn and L. J. Sham, Phys. Rev. **140**, A1133 (1965), ISSN 0031-899X, URL <http://link.aps.org/doi/10.1103/PhysRev.140.A1133>.
- [3] A. D. Becke, J. Chem. Phys. **140**, 18A301 (2014), ISSN 1089-7690, URL <http://www.ncbi.nlm.nih.gov/pubmed/24832308>.
- [4] R. O. Jones, Rev. Mod. Phys. **87**, 897 (2015), ISSN 0034-6861, URL <http://link.aps.org/doi/10.1103/RevModPhys.87.897>.
- [5] N. Mardirossian and M. Head-Gordon, Mol. Phys. **115**, 2315 (2017), ISSN 0026-8976, URL <http://dx.doi.org/10.1080/00268976.2017.1333644><https://www.tandfonline.com/doi/full/10.1080/00268976.2017.1333644>.
- [6] S. Lehtola, arXiv p. 1902.01431 (2019), 1902.01431, URL <http://arxiv.org/abs/1902.01431>.

- [7] S. Lehtola, J. Chem. Theory Comput. p. acs.jctc.8b01089 (2019), ISSN 1549-9618, 1810.11659, URL <http://arxiv.org/abs/1810.11659><http://pubs.acs.org/doi/10.1021/acs.jctc.8b01089>.
- [8] S. Lehtola, *HelFEM – Finite element methods for electronic structure calculations on small systems* (2018), URL <http://github.com/susilehtola/HelFEM>.
- [9] S. Lehtola, C. Steigemann, M. J. Oliveira, and M. A. Marques, SoftwareX **7**, 1 (2018), ISSN 23527110, URL <http://linkinghub.elsevier.com/retrieve/pii/S2352711017300602><https://linkinghub.elsevier.com/retrieve/pii/S2352711017300602>.
- [10] A. D. Becke, J. Chem. Phys. **98**, 1372 (1993), ISSN 0021-9606, URL <http://link.aip.org/link/JCPSA6/v98/i2/p1372/s1&Agg=doi><http://aip.scitation.org/doi/10.1063/1.464304>.
- [11] D. Langreth and J. Perdew, Phys. Rev. B **21**, 5469 (1980), ISSN 0163-1829, URL <http://link.aps.org/doi/10.1103/PhysRevB.21.5469>.
- [12] J. Perdew, S. Kurth, A. Zupan, and P. Blaha, Phys. Rev. Lett. **82**, 2544 (1999), ISSN 0031-9007, URL <http://link.aps.org/doi/10.1103/PhysRevLett.82.5179><http://link.aps.org/doi/10.1103/PhysRevLett.82.2544>.
- [13] P. Pulay, Chem. Phys. Lett. **73**, 393 (1980), ISSN 00092614, URL <http://linkinghub.elsevier.com/retrieve/pii/0009261480803964>.
- [14] P. Pulay, J. Comput. Chem. **3**, 556 (1982), ISSN 0192-8651, URL <http://doi.wiley.com/10.1002/jcc.540030413>.
- [15] X. Hu and W. Yang, J. Chem. Phys. **132**, 054109 (2010), ISSN 1089-7690, URL <http://www.pubmedcentral.nih.gov/articlerender.fcgi?artid=2830258&tool=pmcentrez&rendertype=abstract>.
- [16] S. Lehtola, *ERKALE – HF/DFT from Hel* (2018), URL <https://github.com/susilehtola/erkale>.
- [17] J. Lehtola, M. Hakala, A. Sakko, and K. Hämmäläinen, J. Comput. Chem. **33**, 1572 (2012), ISSN 01928651, URL <http://doi.wiley.com/10.1002/jcc.22987>.
- [18] R. M. Parrish, L. A. Burns, D. G. A. Smith, A. C. Simmonett, A. E. DePrince, E. G. Hohenstein, U. Bozkaya, A. Y. Sokolov, R. Di Remigio, R. M. Richard, et al., J. Chem. Theory Comput. **13**, 3185 (2017), ISSN 1549-9618, URL <http://pubs.acs.org/doi/abs/10.1021/acs.jctc.7b00174><http://pubs.acs.org/doi/10.1021/acs.jctc.7b00174>.
- [19] Q. Sun, T. C. Berkelbach, N. S. Blunt, G. H. Booth, S. Guo, Z. Li, J. Liu, J. D. McClain, E. R. Sayfutyarova, S. Sharma, et al., Wiley Interdiscip. Rev. Comput. Mol. Sci. **8**, e1340 (2018), ISSN 17590876, 1701.08223, URL <http://doi.wiley.com/10.1002/wcms.1340>.

- [20] P. Schwerdtfeger, in *Atoms, Mol. Clust. Electr. Fields* (Published by Imperial College Press and distributed by World Scientific Publishing Co., 2006), pp. 1–32, URL http://www.worldscientific.com/doi/abs/10.1142/9781860948862_0001.
- [21] P. Schwerdtfeger and J. K. Nagle, *Mol. Phys.* **0**, 1 (2018), ISSN 0026-8976, URL <https://www.tandfonline.com/doi/full/10.1080/00268976.2018.1535143>.
- [22] A. Vela and J. L. Gazquez, *J. Am. Chem. Soc.* **112**, 1490 (1990), ISSN 0002-7863, URL <http://pubs.acs.org/doi/abs/10.1021/ja00160a029>.
- [23] T. K. Ghanty and S. K. Ghosh, *J. Phys. Chem.* **100**, 12295 (1996), ISSN 0022-3654, URL <http://pubs.acs.org/doi/abs/10.1021/jp960276m>.
- [24] U. Hohm, *J. Phys. Chem. A* **104**, 8418 (2000), ISSN 1089-5639, URL <http://pubs.acs.org/doi/abs/10.1021/jp0014061>.
- [25] B. Gómez, P. Fuentealba, and R. Contreras, *Theor. Chem. Accounts Theory, Comput. Model. (Theoretica Chim. Acta)* **110**, 421 (2003), ISSN 1432-881X, URL <http://link.springer.com/10.1007/s00214-003-0497-4>.
- [26] P. Calaminici, K. Jug, and A. M. Köster, *J. Chem. Phys.* **109**, 7756 (1998), ISSN 0021-9606, URL <http://scitation.aip.org/content/aip/journal/jcp/109/18/10.1063/1.477421><http://aip.scitation.org/doi/10.1063/1.477421>.
- [27] P. Sałek, T. Helgaker, O. Vahtras, H. Ågren, D. Jonsson, and J. Gauss, *Mol. Phys.* **103**, 439 (2005), ISSN 0026-8976, URL <http://www.tandfonline.com/doi/abs/10.1080/00268970412331319254>.
- [28] K. Y. Suponitsky, S. Tafur, and A. E. Masunov, *J. Chem. Phys.* **129**, 044109 (2008), ISSN 0021-9606, URL <http://aip.scitation.org/doi/10.1063/1.2936121>.
- [29] D. Hait and M. Head-Gordon, *Phys. Chem. Chem. Phys.* **20**, 19800 (2018), ISSN 1463-9076, URL <http://pubs.rsc.org/en/Content/ArticleLanding/2018/CP/C8CP03569E><http://xlink.rsc.org/?DOI=C8CP03569E>.
- [30] P. Fuentealba and Y. Simón-Manso, *J. Phys. Chem. A* **101**, 4231 (1997), ISSN 1089-5639, URL <http://pubs.acs.org/doi/abs/10.1021/jp963903g>.
- [31] T. Voegel, J. Hinze, and F. Tobin, *J. Chem. Phys.* **70**, 1107 (1979), ISSN 0021-9606, URL <http://aip.scitation.org/doi/10.1063/1.437610>.
- [32] J. Stiehler and J. Hinze, *J. Phys. B At. Mol. Opt. Phys.* **28**, 4055 (1995), ISSN 0953-4075, URL <http://stacks.iop.org/0953-4075/28/i=18/a=010?key=crossref.ce3993fe9287050806b0f4cc9c351e25>.
- [33] V. Koch and D. Andrae, *Int. J. Quantum Chem.* **111**, 891 (2011), ISSN 00207608, URL <http://www.ncbi.nlm.nih.gov/pubmed/22667544%5Cnhttp://link.aip.org/link/JCPSA6/v109/i23/p10180/s1&Agg=doi%5Cnhttp://www.pubmedcentral.nih.gov/articlerender.fcgi?artid=2629592&tool=pmcentrez&rendertype=abstract%5Cnhttp://link.aps.org/doi/10.1103/PhysRevA.7>.

- [34] V. Koch and D. Andrae, *Eur. Phys. J. D* **67**, 139 (2013), ISSN 1434-6060, URL <http://link.springer.com/10.1140/epjd/e2013-40191-5>.
- [35] R. M. Dickson and A. D. Becke, *J. Phys. Chem.* **100**, 16105 (1996), ISSN 0022-3654, URL <http://pubs.acs.org/doi/abs/10.1021/jp9605966>.
- [36] D. E. Woon and T. H. Dunning, *J. Chem. Phys.* **100**, 2975 (1994), ISSN 00219606, URL <http://scitation.aip.org/content/aip/journal/jcp/100/4/10.1063/1.466439>.
- [37] P. Soldán, E. P. F. Lee, and T. G. Wright, *Phys. Chem. Chem. Phys.* **3**, 4661 (2001), ISSN 1463-9076, URL <http://xlink.rsc.org/?DOI=b105433n>.
- [38] R. Bast, A. Heßelmann, P. Salek, T. Helgaker, and T. Saue, *ChemPhysChem* **9**, 445 (2008), ISSN 14394235, URL <http://doi.wiley.com/10.1002/cphc.200700504>.
- [39] P. Parmar, K. A. Peterson, and A. E. Clark, *J. Phys. Chem. A* **117**, 11874 (2013), ISSN 1089-5639, URL <http://pubs.acs.org/doi/10.1021/jp403078j>.
- [40] P. Parmar, K. A. Peterson, and A. E. Clark, *J. Chem. Phys.* **141**, 234304 (2014), ISSN 0021-9606, URL <http://aip.scitation.org/doi/10.1063/1.4903792>.
- [41] J. Kobus, *Phys. Rev. A* **91**, 022501 (2015), ISSN 1050-2947, URL <https://link.aps.org/doi/10.1103/PhysRevA.91.022501>.
- [42] F. Bloch, *Zeitschrift für Phys.* **57**, 545 (1929), ISSN 1434-6001, URL <http://link.springer.com/10.1007/BF01340281>.
- [43] P. A. M. Dirac, *Math. Proc. Cambridge Philos. Soc.* **26**, 376 (1930), ISSN 0305-0041, URL http://www.journals.cambridge.org/abstract_S0305004100016108.
- [44] J. P. Perdew and Y. Wang, *Phys. Rev. B* **45**, 13244 (1992), ISSN 0163-1829, URL <http://link.aps.org/doi/10.1103/PhysRevB.45.13244>.
- [45] J. P. Perdew, K. Burke, and M. Ernzerhof, *Phys. Rev. Lett.* **77**, 3865 (1996), ISSN 0031-9007, URL <http://www.ncbi.nlm.nih.gov/pubmed/22502509><http://link.aps.org/doi/10.1103/PhysRevLett.77.3865>.
- [46] J. P. Perdew, K. Burke, and M. Ernzerhof, *Phys. Rev. Lett.* **78**, 1396 (1997), ISSN 0031-9007, URL <http://link.aps.org/doi/10.1103/PhysRevLett.78.1396>.
- [47] C. Adamo and V. Barone, *J. Chem. Phys.* **110**, 6158 (1999), ISSN 0021-9606, URL <http://link.aip.org/link/JCPSA6/v110/i13/p6158/s1&Agg=doihttp://aip.scitation.org/doi/10.1063/1.478522>.
- [48] M. Ernzerhof and G. E. Scuseria, *J. Chem. Phys.* **110**, 5029 (1999), ISSN 0021-9606, URL <http://link.aip.org/link/JCPSA6/v110/i11/p5029/s1&Agg=doihttp://aip.scitation.org/doi/10.1063/1.478401>.

- [49] J. Tao, J. P. Perdew, V. N. Staroverov, and G. E. Scuseria, Phys. Rev. Lett. **91**, 146401 (2003), ISSN 0031-9007, URL <http://link.aps.org/doi/10.1103/PhysRevLett.91.146401>.
- [50] J. P. Perdew, J. Tao, V. N. Staroverov, and G. E. Scuseria, J. Chem. Phys. **120**, 6898 (2004), ISSN 0021-9606, URL <http://www.ncbi.nlm.nih.gov/pubmed/15267588>.
- [51] V. N. Staroverov, G. E. Scuseria, J. Tao, and J. P. Perdew, J. Chem. Phys. **119**, 12129 (2003), ISSN 00219606, URL <http://link.aip.org/link/JCPA6/v119/i23/p12129/s1&Agg=doi>.
- [52] J. M. Galbraith and H. F. Schaefer, J. Chem. Phys. **105**, 862 (1996), ISSN 0021-9606, URL <http://aip.scitation.org/doi/10.1063/1.471933>.
- [53] N. Rösch and S. B. Trickey, J. Chem. Phys. **106**, 8940 (1997), ISSN 0021-9606, URL <http://aip.scitation.org/doi/10.1063/1.473946>.
- [54] A. A. Jarecki and E. R. Davidson, Chem. Phys. Lett. **300**, 44 (1999), ISSN 00092614, URL <http://linkinghub.elsevier.com/retrieve/pii/S0009261498013670>.
- [55] F. Jensen, J. Chem. Theory Comput. **6**, 2726 (2010), ISSN 1549-9618, URL <http://pubs.acs.org/doi/abs/10.1021/ct1003324>.
- [56] L. N. Anderson, M. B. Oviedo, and B. M. Wong, J. Chem. Theory Comput. **13**, 1656 (2017), ISSN 1549-9618, URL <http://pubs.acs.org/doi/10.1021/acs.jctc.6b01249>.
- [57] F. Jensen, Theor. Chem. Acc. **126**, 371 (2010), ISSN 1432-881X, URL <http://link.springer.com/10.1007/s00214-009-0699-5>.
- [58] S. Lehtola, arXiv p. 1810.11653 (2018), 1810.11653, URL <http://arxiv.org/abs/1810.11653>.
- [59] R. Ram-Mohan, *Finite Element and Boundary Element Applications in Quantum Mechanics* (Oxford University Press Inc., New York, New York, 2002), ISBN 9780198525219, URL <https://global.oup.com/academic/product/finite-element-and-boundary-element-applications-in-quantum-mechanics-9780198525219>.
- [60] L. R. Ram-Mohan, S. Saigal, D. Dossa, and J. Shertzer, Comput. Phys. **4**, 50 (1990), ISSN 08941866, URL <http://scitation.aip.org/content/aip/journal/cip/4/1/10.1063/1.168374>.
- [61] A. T. Patera, J. Comput. Phys. **54**, 468 (1984), ISSN 00219991, URL <http://linkinghub.elsevier.com/retrieve/pii/0021999184901281>.
- [62] J. R. Flores, E. Clementi, and V. Sonnad, J. Chem. Phys. **91**, 7030 (1989), ISSN 0021-9606, URL <http://aip.scitation.org/doi/10.1063/1.457320>.

- [63] J. Flores, E. Clementi, and V. Sonnad, *Chem. Phys. Lett.* **163**, 198 (1989), ISSN 00092614, URL <http://linkinghub.elsevier.com/retrieve/pii/000926148980034X>.
- [64] C. Froese Fischer, W. Guo, and Z. Shen, *Int. J. Quantum Chem.* **42**, 849 (1992), ISSN 0020-7608, URL <http://doi.wiley.com/10.1002/qua.560420422>.
- [65] C. Roothaan, *Rev. Mod. Phys.* **23**, 69 (1951), ISSN 0034-6861, URL <http://link.aps.org/doi/10.1103/RevModPhys.23.69>.
- [66] J. A. Pople and R. K. Nesbet, *J. Chem. Phys.* **22**, 571 (1954), ISSN 00219606, URL <http://link.aip.org/link/JCPA6/v22/i3/p571/s1&Agg=doi>.
- [67] J. A. Pople, P. M. W. Gill, and B. G. Johnson, *Chem. Phys. Lett.* **199**, 557 (1992), ISSN 00092614, URL <http://linkinghub.elsevier.com/retrieve/pii/000926149285009Y>.
- [68] R. Neumann, R. H. Nobes, and N. C. Handy, *Mol. Phys.* **87**, 1 (1996), ISSN 0026-8976, URL <http://journalsonline.tandf.co.uk/Index/10.1080/00268979650027630>.
- [69] N. S. Ostlund, *J. Chem. Phys.* **57**, 2994 (1972), ISSN 00219606, URL <http://link.aip.org/link/?JCP/57/2994/1&Agg=doi>.
- [70] W. D. Edwards, *Int. J. Quantum Chem.* **34**, 549 (1988), ISSN 0020-7608, URL <http://doi.wiley.com/10.1002/qua.560340859>.
- [71] S. Lehtola and H. Jónsson, *J. Chem. Theory Comput.* **10**, 5324 (2014), ISSN 1549-9618, URL <http://pubs.acs.org/doi/abs/10.1021/ct500637x>.
- [72] D. W. Small, E. J. Sundstrom, and M. Head-Gordon, *J. Chem. Phys.* **024104** (2015), ISSN 0021-9606.
- [73] S. Lehtola, M. Head-Gordon, and H. Jónsson, *J. Chem. Theory Comput.* **12**, 3195 (2016), ISSN 1549-9618, URL <http://pubs.acs.org/doi/abs/10.1021/acs.jctc.6b00347>.
- [74] S. Lehtola, E. Ö. Jónsson, and H. Jónsson, *J. Chem. Theory Comput.* **12**, 4296 (2016), ISSN 1549-9618, URL <http://pubs.acs.org/doi/abs/10.1021/acs.jctc.6b00622>.
- [75] S. Lehtola, M. Dimitrova, and D. Sundholm, arXiv p. 1812.06274 (2018), 1812.06274, URL <http://arxiv.org/abs/1812.06274>.
- [76] P.-O. Löwdin, *J. Chem. Phys.* **18**, 365 (1950), ISSN 00219606, URL <http://link.aip.org/link/JCPA6/v18/i3/p365/s1&Agg=doi>.
- [77] J. Lehtola, M. Hakala, J. Vaara, and K. Hämmäläinen, *Phys. Chem. Chem. Phys.* **13**, 5630 (2011), ISSN 1463-9084, URL <http://pubs.rsc.org/en/content/articlehtml/2011/cp/c0cp02269a><http://www.ncbi.nlm.nih.gov/pubmed/21283842>.

- [78] S. Huzinaga, *Prog. Theor. Phys.* **15**, 501 (1956), ISSN 0033-068X, URL <http://ptp.oxfordjournals.org/content/15/5/501.short%5Cnhttp://ptp.oxfordjournals.org/cgi/doi/10.1143/PTP.15.501><https://academic.oup.com/ptp/article-lookup/doi/10.1143/PTP.15.501>.
- [79] D. M. Bishop, *Adv. Quantum Chem.* **3**, 25 (1967), ISSN 00653276.
- [80] J. P. Desclaux, in *Relativ. Eff. Atoms, Mol. Solids* (Springer US, Boston, MA, 1983), pp. 213–225, URL http://link.springer.com/10.1007/978-1-4613-3596-2_10.
- [81] S.-L. Hu, Z.-X. Zhao, and T.-Y. Shi, *Int. J. Quantum Chem.* **114**, 441 (2014), ISSN 00207608, URL <http://doi.wiley.com/10.1002/qua.24582>.
- [82] C. W. Murray, N. C. Handy, and G. J. Laming, *Mol. Phys.* **78**, 997 (1993), ISSN 0026-8976, URL <http://www.tandfonline.com/doi/abs/10.1080/00268979300100651>.
- [83] V. Lebedev, *USSR Comput. Math. Math. Phys.* **15**, 44 (1975), ISSN 00415553, URL <http://linkinghub.elsevier.com/retrieve/pii/0041555375901330>.
- [84] V. Lebedev, *USSR Comput. Math. Math. Phys.* **16**, 10 (1976), ISSN 00415553, URL <http://linkinghub.elsevier.com/retrieve/pii/0041555376901002>.
- [85] T. Leininger, H. Stoll, H.-J. Werner, and A. Savin, *Chem. Phys. Lett.* **275**, 151 (1997), ISSN 00092614, URL <http://linkinghub.elsevier.com/retrieve/pii/S0009261497007586>.
- [86] T. Yanai, D. P. Tew, and N. C. Handy, *Chem. Phys. Lett.* **393**, 51 (2004), ISSN 00092614, URL <http://linkinghub.elsevier.com/retrieve/pii/S0009261404008620>.
- [87] R. Peverati and D. G. Truhlar, *J. Phys. Chem. Lett.* **2**, 2810 (2011), ISSN 1948-7185, URL <http://pubs.acs.org/doi/abs/10.1021/jz201170d>.
- [88] R. Peverati and D. G. Truhlar, *Phys. Chem. Chem. Phys.* **14**, 16187 (2012), ISSN 1463-9084, URL <http://www.ncbi.nlm.nih.gov/pubmed/23132141>.
- [89] J.-D. Chai and M. Head-Gordon, *J. Chem. Phys.* **128**, 084106 (2008), ISSN 0021-9606, URL <http://www.ncbi.nlm.nih.gov/pubmed/18315032>.
- [90] N. Mardirossian and M. Head-Gordon, *Phys. Chem. Chem. Phys.* **16**, 9904 (2014), ISSN 1463-9084.
- [91] N. Mardirossian and M. Head-Gordon, *J. Chem. Phys.* **144**, 214110 (2016), ISSN 0021-9606, URL <http://scitation.aip.org/content/aip/journal/jcp/144/21/10.1063/1.4952647>.
- [92] R. D. Adamson, J. P. Dombroski, and P. M. W. Gill, *J. Comput. Chem.* **20**, 921 (1999), ISSN 0192-8651, URL [http://doi.wiley.com/10.1002/\(SICI\)1096-987X\(19990715\)20:9%3C921::AID-JCC3%3E3.0.CO;2-K](http://doi.wiley.com/10.1002/(SICI)1096-987X(19990715)20:9%3C921::AID-JCC3%3E3.0.CO;2-K).

- [93] R. Ahlrichs, *Phys. Chem. Chem. Phys.* **8**, 3072 (2006), ISSN 1463-9076, URL <http://www.ncbi.nlm.nih.gov/pubmed/16804606>.
- [94] C. Sanderson and R. Curtin, *J. Open Source Softw.* **1**, 26 (2016), ISSN 2475-9066, /dx.doi.org/10.21105/joss.00026, URL <http://joss.theoj.org/papers/10.21105/joss.00026>.
- [95] C. Sanderson and R. Curtin, in *ICMS 2018 Math. Softw. – ICMS 2018*, edited by J. Davenport, M. Kauers, G. Labahn, and J. Urban (Springer, Cham, 2018), pp. 422–430, ISBN 978-3-319-96418-8, URL http://link.springer.com/10.1007/978-3-319-96418-8_50.
- [96] T. Tsuchimochi and G. E. Scuseria, *J. Chem. Phys.* **133**, 141102 (2010), ISSN 1089-7690, URL <http://www.ncbi.nlm.nih.gov/pubmed/20949979>.
- [97] T. Tsuchimochi and G. E. Scuseria, *J. Chem. Phys.* **134**, 064101 (2011), ISSN 1089-7690, URL <http://www.ncbi.nlm.nih.gov/pubmed/21322655>.
- [98] J. L. Gázquez and H. J. Silverstone, *J. Chem. Phys.* **67**, 1887 (1977), ISSN 00219606, URL <http://scitation.aip.org/content/aip/journal/jcp/67/5/10.1063/1.435119>.
- [99] C. Froese, *Can. J. Phys.* **41**, 1895 (1963), ISSN 0008-4204, URL <http://www.nrcresearchpress.com/doi/10.1139/p63-189>.
- [100] S. L. Saito, *Theor. Chem. Accounts Theory, Comput. Model. (Theoretica Chim. Acta)* **109**, 326 (2003), ISSN 1432-881X, URL <http://link.springer.com/10.1007/s00214-003-0437-3>.
- [101] C. Froese Fischer, *Comput. Phys. Commun.* **182**, 1315 (2011), ISSN 00104655, URL <http://linkinghub.elsevier.com/retrieve/pii/S0010465511000324>.
- [102] Z. Romanowski, *Mol. Phys.* **107**, 1339 (2009), ISSN 0026-8976, URL <http://www.tandfonline.com/doi/abs/10.1080/00268970902873554>.
- [103] S. L. Saito, *At. Data Nucl. Data Tables* **95**, 836 (2009), ISSN 0092640X, URL <http://dx.doi.org/10.1016/j.adt.2009.06.001>.
- [104] W. Schweizer, P. Faßbinder, R. González-Ferez, M. Braun, S. Kulla, and M. Stehle, *J. Comput. Appl. Math.* **109**, 95 (1999), ISSN 03770427, URL <http://linkinghub.elsevier.com/retrieve/pii/S0377042799001557>.
- [105] P. Motamarri, M. Nowak, K. Leiter, J. Knap, and V. Gavini, *J. Comput. Phys.* **253**, 308 (2013), ISSN 00219991, 1207.0167, URL <http://dx.doi.org/10.1016/j.jcp.2013.06.042><http://linkinghub.elsevier.com/retrieve/pii/S0021999113004774>.
- [106] P. Lykos and G. W. Pratt, *Rev. Mod. Phys.* **35**, 496 (1963), ISSN 0034-6861, URL <https://link.aps.org/doi/10.1103/RevModPhys.35.496>.

- [107] R. F. Prat, Phys. Rev. A **6**, 1735 (1972), ISSN 0556-2791, URL <https://link.aps.org/doi/10.1103/PhysRevA.6.1735>.
- [108] R. Seeger and J. A. Pople, J. Chem. Phys. **66**, 3045 (1977), ISSN 0021-9606, URL <http://link.aip.org/link/JCPSA6/v66/i7/p3045/s1&Agg=doi><http://aip.scitation.org/doi/10.1063/1.434318>.
- [109] R. Bauernschmitt and R. Ahlrichs, J. Chem. Phys. **104**, 9047 (1996), ISSN 00219606, URL <http://link.aip.org/link/JCPSA6/v104/i22/p9047/s1&Agg=doi>.
- [110] T. Koga, E. Shibata, and A. J. Thakkar, Theor. Chim. Acta **91**, 47 (1995), ISSN 0040-5744, URL <http://link.springer.com/10.1007/BF01113861>.
- [111] T. Koga and A. J. Thakkar, J. Phys. B At. Mol. Opt. Phys. **29**, 2973 (1996), ISSN 0953-4075, URL <http://stacks.iop.org/0953-4075/29/i=14/a=010?key=crossref.a541bee3978180a2b3d5cfcb72687eb2>.